

Effects of temperature on asexual reproduction and jellyfish booms of *Aurelia aurita*: Insights from mathematical modeling

Wei Wang^a, Mengjie Wang^a, Hao Wang^{b,*}

^a College of Mathematics and Systems Science, Shandong University of Science and Technology, Qingdao 266590, China

^b Department of Mathematical and Statistical Sciences, University of Alberta, Edmonton, AB T6G 2G1, Canada

ARTICLE INFO

Keywords:

Aurelia aurita
PSEM dynamic model
Life history
Temperature
Strobila

ABSTRACT

Elucidating the benthic stage growth and reproductive mechanisms of *Aurelia aurita* contributes to understanding irregular jellyfish blooms. This paper establishes a four-stage life history model of *A. aurita* (Polyp–Strobila–Ephyra–Medusa) to investigate the influence of seasonal temperature variations on the abundance of *A. aurita*. Sensitivity analyses indicate that jellyfish are most sensitive to bottom-up supplementation, with strobilation identified as an essential process in their life cycle. We explore the effects of parameters directly associated with strobilation in the Jiaozhou Bay area on population size, summarizing the interannual variations across the four stages of *A. aurita*, which aligns with empirical data. The investigation reveals that (i) consistent with recent biological literature, strobilation of *A. aurita* in temperate regions primarily occurs during periods of increasing spring sea surface temperatures rather than during autumn temperature declines, leading to summer jellyfish blooms; (ii) regression and subsequent strobilation favor an increase in the pelagic medusae population; (iii) the influence of rising sea surface temperatures due to climate change on the growth and reproduction of *A. aurita* manifests as initial stimulation followed by inhibition; (iv) earlier strobilation in spring may lead to more extensive *A. aurita* outbreaks in summer, providing insights for early warning of jellyfish blooms.

1. Introduction

The common moon jellyfish, *Aurelia aurita* (Scyphozoa), is a widely distributed and abundant species of jellyfish (Purcell et al., 2007). The abundance of jellyfish populations fluctuates on decadal scales in response to climate cycles (Condon et al., 2013; Purcell, 2005). However, with increasing human activities along coastlines, the intensity and frequency of jellyfish blooms are also on the rise (Condon et al., 2013; Duarte et al., 2013; Kogovšek et al., 2010), leading to significant ecological and socio-economic impacts in tourism, coastal services, marine fisheries, planktonic and fish community structures, and human safety, garnering widespread attention (Chi et al., 2022; Condon et al., 2013; Fuentes et al., 2018; Tiller et al., 2017; Zheng et al., 2010).

Understanding the life history of *A. aurita* is crucial for predicting and controlling its outbreaks (Zheng et al., 2010). The life cycle of Scyphozoa jellyfish typically consists of three stages: the swimming non-feeding larva, the long-lived sessile polyp, and the free-swimming medusa stage (Kraus et al., 2015) (see Fig. 1.1). Jellyfish populations are regulated via a bottom-up process (Purcell, 2012). The ontogeny, maturation, and fecundity of benthic stages, modulated by various interacting factors (Benedetti-Cecchi et al., 2015; Li and Liu, 2022),

play a fundamental role in the dynamics of the pelagic adult medusae populations (Han and Uye, 2010; Purcell et al., 2009; Willcox et al., 2008; Zang et al., 2023).

Two primary classifications exist for external natural factors influencing benthic stage population dynamics. The first is biological factors, such as interactions between benthic organisms significantly affecting polyps (Feng et al., 2017; Miyake et al., 2002; Schiariti et al., 2015; Zang et al., 2023), and interspecific relationships like predation and competition impacting polyp abundance (Hernroth and Gröndahl, 1985; Hoover et al., 2012; Takao et al., 2014). The second type includes other environmental factors like temperature, salinity, dissolved oxygen concentration, light availability, food supply, substrate type, etc., where temperature and substrate type are considered significantly correlated with jellyfish abundance (Ishii et al., 2008; Zang et al., 2023).

Furthermore, anthropogenic factors such as climate change, eutrophication, overfishing, aquaculture, marine construction, and species invasions may favor jellyfish reproduction (Purcell et al., 2007). The physiological and reproductive characteristics of jellyfish enable them to adapt to various environmental conditions, such as hypoxia and starvation, allowing jellyfish populations to thrive even when human

* Corresponding author.

E-mail addresses: weiwang10437@sdust.edu.cn (W. Wang), mengjiawang@sdust.edu.cn (M. Wang), hao8@ualberta.ca (H. Wang).

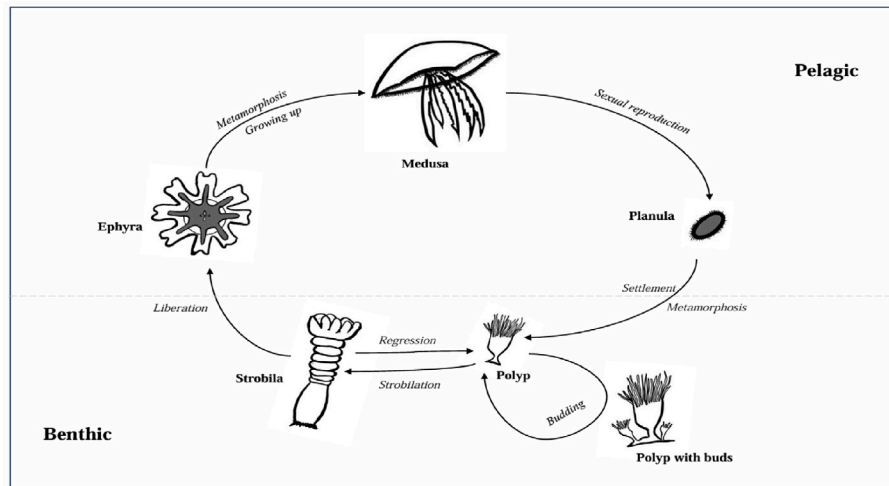


Fig. 1.1. Life cycle of *Aurelia aurita*. Medusae engage in sexual reproduction, giving rise to minute planula larvae that settle on a firm substrate at the base and undergo metamorphosis into polyps. Polyps reproduce asexually through the budding of lateral clones (Treible and Condon, 2019). Under specific environmental conditions, polyps initiate metamorphosis and strobilation. Each strobila has the capacity to generate multiple ephyrae, which are released into the water and mature into free-swimming medusae. Concurrently, strobilae that have released all ephyrae regress into polyps, capable of budding or undergoing fission once more (Cabral-Arellano et al., 2017).

activities are detrimental to other marine organisms, leading to the preservation or expansion of jellyfish populations (Dong et al., 2019; Ishii and Katsukoshi, 2010; Roveta et al., 2022; Wang et al., 2015; Zang et al., 2023).

Some researchers have applied empirical methods to study benthic polyp stage population dynamics (Purcell et al., 2007; Willcox et al., 2008). Ruiz et al. developed a life history model to explore the biological and statistical impacts (Ruiz et al., 2012). However, conclusions drawn from experiments and statistical models in specific regions are insufficient to represent the mechanisms of the entire species (Yu et al., 2023). Fewer studies have established dynamic models for the entire pelagic–benthic life cycle to elucidate long-term jellyfish dynamics (Li and Liu, 2022; Xie et al., 2015). Xie et al. introduce a Polyp–Medusa model for Scyphozoa and confirmed that the expansion of substrates exerts a more pronounced influence on population dynamics (Xie et al., 2015). Nevertheless, the growth, reproduction, and mortality rates driven by consumption are not considered. Henschke et al. elaborate on these aspects and find that their findings align closely with empirical observations (Henschke et al., 2018). Furthermore, Goldstein and Steiner introduce a stage-structured matrix population model and demonstrate that heightened food availability may be a crucial ecological driver for jellyfish blooms (Goldstein and Steiner, 2020). Some scholars present individual-based models (IBM) to assess the interplay between the physical dispersal of jellyfish and their biological behaviors, which typically necessitates a substantial amount of empirical data for model parameter calibration and demands significant computational resources (Li and Liu, 2022; Rahi et al., 2020). The essential podocyst dormancy of certain jellyfish is illuminated by the model proposed by Xie et al. (2021), yet its applicability remains limited to a broader range of species. Yu et al. building upon (Xie et al., 2015), develop a triphasic (Medusa–Polyp–Ephyra) life cycle model for *A. aurita*, revealing a significant influence of strobilation on the population size of jellyfish (Yu et al., 2023).

Strobilation can be divided into three stages in experimental settings: pre-strobilation, bet-strobilation, and strobilation stages (Xing et al., 2020). During the bet-strobilation and strobilation stages, jellyfish are in the strobila phase, whereas in the pre-strobilation stage, jellyfish remain in the polyp form. The physiological and reproductive characteristics of polyps and strobila differ significantly, and each of both adapts to different environments (Willcox et al., 2008). Environmental factors, such as temperature and food supply, can influence the decision-making process of a polyp to either bud more polyps or undergo strobilation. When temperatures are high, polyps

tend to bud more individuals to expand population size, whereas, at low temperatures and food concentrations, polyps transition from budding reproduction to strobilation, allowing them to escape unfavorable conditions, followed by sexual reproduction to expand habitats and enhance genetic diversity (Chi et al., 2022; Gerber et al., 2018). Additionally, Chi et al. (2022) indicates that temperature variations correspond to different strobilation rates, highlighting the sensitivity of strobila to temperature changes. Thus, as the success of strobilation directly determines the recruitment of the medusa population (Chi et al., 2022; Lucas et al., 2012), it is essential to study strobila as a separate stage.

Inspired by above works, in this paper, a PSEM (Polyp–Strobila–Ephyra–Medusa) model is suggested to depict the effects of temperature variations and seasonal fluctuations on the population dynamics of *A. aurita* in temperate regions. Subsequently, sensitivity analyses (SAs) is utilized to identify the critical parameters influencing population size and to propose strategies for managing the jellyfish population. Additionally, we predicted the annual variations in the *A. aurita* population in Jiaozhou Bay against the backdrop of global warming.

2. Methods

2.1. Model formulation

The scyphozoan *Aurelia aurita* exhibits a complex life history, alternating between the stages of swimming larvae, benthic polyps, and pelagic medusae (see Fig. 1.1). For a quantitative characterization of the life cycle traits of *A. aurita* and an investigation into the impact of environmental variables, a dynamic model is formulated under the following assumptions:

- (1) Planula represents the larval stage of the polyp (Gröndahl, 1989), where the number of surviving planula equals the number of polyps generated through medusa's sexual reproduction.
- (2) The life cycle is simplified into four main stages: polyp, strobila, ephyra, and medusa, with polyp and strobila belonging to the benthic stage and ephyra and medusa belonging to the pelagic stage.
- (3) All stages of the life cycle are significantly influenced by temperature (Yu et al., 2023).
- (4) The marine environment is sufficiently large, providing ample food resources for jellyfish growth.

- (5) The polyp is perennial, assuming that under the same temperature, different generations of polyps multiply at a constant rate (Chi et al., 2022).
- (6) Let $P(t)$, $S(t)$, $E(t)$, and $M(t)$ represent the population sizes of polyps, strobilae, ephyrae, and medusae at time t .

The augmentation of polyp population size arises from three factors: asexual reproduction, medusa sexual reproduction, and strobilia regression, whereas the decline in polyp numbers can be ascribed to polyp mortality (natural expiration and entombment under silt or predation by nudibranchs) $\mu_1 P$, as well as intraspecific competition for substrates dP^2 . The asexual reproduction of *A. aurita* is predominantly by budding. Although polyps can also asexually produce stolons, which generate fully active polyps, the occurrence frequency of stolon formation is much lower than that of budding, almost negligible (Han and Uye, 2010). Let η be the sexual reproduction rate and γ be the survival proportion of planula, then $\gamma\eta M$ represents medusa sexual reproduction. Assumed that the budding rate α , the strobilation proportion κ and the strobila development rate β_2 are all functions of temperature T . Then asexual reproduction and the strobilia regression can be written as $\alpha(T)(1 - \kappa(T))P$ and $\beta_2(T)S$, respectively. So the rate of change for polyp can be expressed as

$$\frac{dP}{dt} = \alpha(T)(1 - \kappa(T))P + \beta_2(T)S + \gamma\eta M - \mu_1 P - dP^2. \quad (2.1)$$

The strobila is developed from polyp. Both polyp and strobila belong to the benthic stage. We believe that intraspecific competition occurs during the settling of the floating planulae colonize the substrate, so intraspecific competition is not considered during the strobila phase. Supposing that the mortality rate of strobila is the same as that of polyps. Assume that the polyp strobilation rate β_1 is a function of T . So the population size of strobilae changes due to polyp strobilation $\beta_1(T)\kappa(T)P$, strobila regression $\beta_2(T)S$, and strobila mortality (natural expiration and entombment under silt or predation by nudibranchs) $\mu_1 S$. Therefore, the rate of change for strobila can be articulated as

$$\frac{dS}{dt} = \beta_1(T)\kappa(T)P - \beta_2(T)S - \mu_1 S. \quad (2.2)$$

Given that both the average released quantity of ephyra ρ and the ephyra developmental rate δ are functions of T . Ephyra population size dynamics are driven by strobila strobilation $\rho(T)\beta_2(T)S$, ephyra maturation into medusa $\delta(T)E$, ephyra mortality encompassing natural death and predation $\mu_2 E$, with medusa mortality represented by μ_3 . The rate of change for ephyra and medusa can be characterized as

$$\frac{dE}{dt} = \rho(T)\beta_2(T)S - \delta(T)E - \mu_2 E, \quad (2.3)$$

and

$$\frac{dM}{dt} = \delta(T)E - \mu_3 M. \quad (2.4)$$

Considering the cyclic temperature fluctuations, we investigated the impact of seasonal changes in the life cycle of *A. aurita*. Following (2.1) (2.2) (2.3) (2.4), we have the nonautonomous model:

$$\begin{cases} \frac{dP}{dt} = \alpha(T(t))(1 - \kappa(T(t)))P + \beta_2(T(t))S + \gamma\eta M - dP^2 - \mu_1 P, \\ \frac{dS}{dt} = \beta_1(T(t))\kappa(T(t))P - \beta_2(T(t))S - \mu_1 S, \\ \frac{dE}{dt} = \rho(T(t))\beta_2(T(t))S - \delta(T(t))E - \mu_2 E, \\ \frac{dM}{dt} = \delta(T(t))E - \mu_3 M, \end{cases} \quad (2.5)$$

where α , κ , β_1 , β_2 , ρ and δ represent temperature-dependent periodic functions indicated as $\alpha(t)$, $\kappa(t)$, $\beta_1(t)$, $\beta_2(t)$, $\rho(t)$ and $\delta(t)$, respectively. The parameters pertaining to the aforementioned model are delineated in Table 2.1.

2.2. Parameter calibration

Parameter calibration forms the basis for conducting numerical analyses. As various experiments were conducted using different units of measurement, we ensured dimensional consistency by normalizing the data with days as a universal reference point. Fitting functions are primarily developed by considering the experimental data obtained in Jiaozhou Bay (Chi et al., 2022; Xing et al., 2020). While the data were accessible in the form of figures, these were first digitized using the Digitizer in Origin 2023b. We assumed that $\alpha(T)$ takes the following form, which was then fit to the data of average bud production in Chi et al. (2022) Figures 3 and 4.

$$\alpha(T) = 0.2816 \exp \left\{ - \left(\frac{T-26.05}{14.3} \right)^2 \right\},$$

where R-square is 0.9323 and SSE is 0.00183. Fig. 2.1(c) illustrates $\alpha(T) \in (0.0306, 0.2811)$, with its highest value observed at 25.47 °C. It is noteworthy that a decrease in asexual reproduction activities is observed when temperatures exceed 27 °C (Duan et al., 2020), which aligns with the findings obtained from the fitting analysis. Similarly, $\beta_1(T)$ is described by $\beta_1(T) = 1/\text{Period}$ from the polyps grow up to strobilae (Xing et al., 2020). Then,

$$\beta_1(T) = 0.01985 \exp \{ -0.06(T - 12.58)^2 \} + 0.02076,$$

where R-square is 0.9995 and SSE is 2.773×10^{-8} . Fig. 2.1(a) displays $\beta_1(T) \in (0.0208, 0.0406)$, with its maximum value observed at 12.51 °C. This observation is consistent with the data obtained from field observations as reported in Wang and Sun (2015) and Xing et al. (2020). $\beta_2(T) = 1/\text{Period}$ from the threshold of strobilae strobilation to the last release of ephyrae (Xing et al., 2020). The fitting function of $\beta_2(T)$ are expressed as

$$\beta_2(T) = 0.08127 \exp \{ -0.42(T - 13.91)^2 \} + 0.05589,$$

We assumed that $\kappa(T)$ takes the following form, which was then fit to the data of strobilation rate (%) in Chi et al. (2022) Figure 2(C).

$$\kappa(T) = 0.8627 \exp \left\{ - \left(\frac{T-12.51}{2.551} \right)^2 \right\},$$

where R-square are 0.9997 and 1, SSE are 4.157×10^{-7} and 1.348×10^{-6} , respectively. Given the positive nature of $\beta_2(T)$ and $\kappa(T)$, we standardized the outcomes to yield $\beta_2(T) \in (0.0559, 0.1372)$ and $\kappa(T) \in (0, 0.8627)$. Fig. 2.1 (b) and (f) illustrate that both curves reach peak values around 13 °C, aligning well with the field observations cited in Shi et al. (2018). $\rho(T)$ and $\delta(T)$ were obtained by

$$\rho(T) = \text{Number of released ephyrae/Number of strobilae},$$

and

$$\delta(T) = 1/\text{Period of the ephyrae development},$$

respectively (Chi et al., 2022; Xing et al., 2020). The fitting function were expressed as

$$\rho(T) = 8.22 \exp \left\{ -22.74 \ln^2 \left(\frac{T}{13.64} \right) + 0.07198 \right\},$$

and

$$\delta(T) = 0.04244 \exp \left\{ - \left(\frac{T-16.94}{3.479} \right)^2 \right\},$$

where R-square are both 1, and SSE are 3.115×10^{-16} and 4.659×10^{-8} , respectively. In Fig. 2.1(e), the range of $\rho(T)$ falls between 0.0720 and 16.2920, with the highest value observed at 13.56 °C. On the other hand, Fig. 2.1(d) displays $\delta(T)$ ranging from 0 to 0.0424, with its peak value occurring at 16.93 °C.

Table 2.1
Parameters of model (2.5).

Param.	Description	Range	Unit	V_0	Source
α	Asexual reproduction rate	0.0306–0.2811	ind m ⁻³ day ⁻¹ P ⁻¹	0.185	Chi et al. (2022)
β_1	Polyp strobilation rate	0.0208–0.0406	day ⁻¹	0.03	Xing et al. (2020)
β_2	Strobila development rate	0.0559–0.1372	day ⁻¹	0.029	Xing et al. (2020)
κ	Polyp strobilation proportion	0–0.8627	–	0.7	Chi et al. (2022)
δ	Ephyra development rate	0–0.0424	day ⁻¹	0.02	Xing et al. (2020)
ρ	Average released quantity of ephyra	0–16.2920	ind m ⁻³ S ⁻¹	12.79	Xing et al. (2020)
η	Sexual reproduction rate	22.88–212.42	ind m ⁻³ day ⁻¹ M ⁻¹	100	Lucas (1996) and Yu et al. (2023)
γ	Survival proportion of planula	0.001–0.3	–	0.004	Cui et al. (2018), Conley and Uye (2015) and Yu et al. (2023)
d	Intraspecific competition among polyps	0–0.037	ind ⁻¹ m ³ day ⁻¹	0.005	Wang (2013), Xie et al. (2015) and Yu et al. (2023)
μ_1	Mortality rate of polyp and strobila	0–0.048	day ⁻¹	0.01	Duan et al. (2020), Wang (2013) and Sun et al. (2017)
μ_2	Mortality rate of ephyra	0–0.083	day ⁻¹	0.01	Wang et al. (2015) and Yu et al. (2023)
μ_3	Mortality rate of medusa	0.0033–0.0082	day ⁻¹	0.0065	Wang (2013) and Yu et al. (2023)

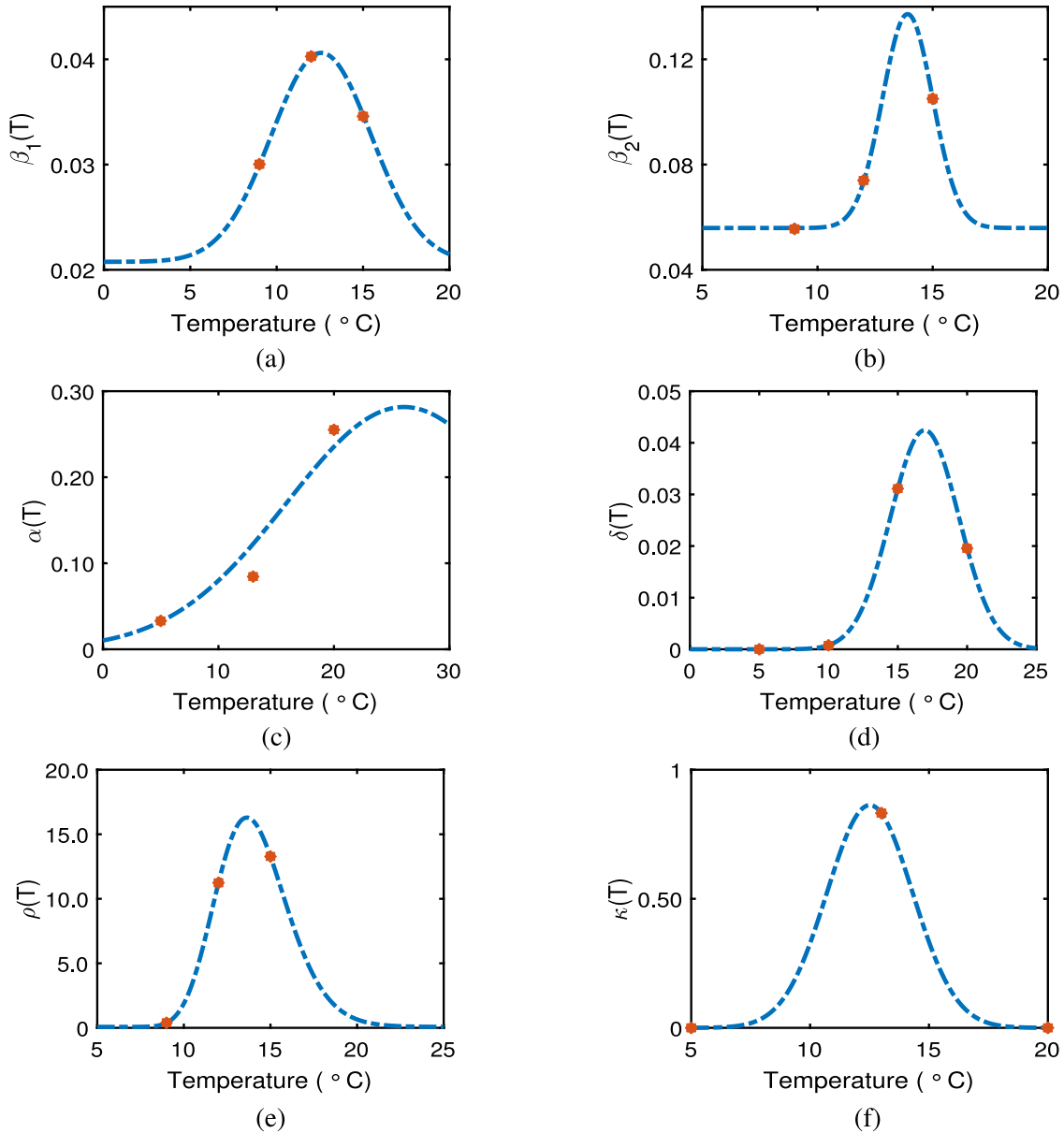


Fig. 2.1. Fitting plots of parameters. (a)–(f) depict the fitted curves of $\beta_1(T)$, $\beta_2(T)$, $\alpha(T)$, $\delta(T)$, $\rho(T)$, and $\kappa(T)$, respectively.

2.3. Sensitivity analyses

Sensitivity analysis, occupying a pivotal position in the model development and enhancement, is precisely designed to identify the

contribution of specific parameters within the model. Numerous approaches are available nowadays to perform sensitivity analyses. In this paper, the Sobol method is utilized to qualitatively assess the parameter sensitivities concerning the internal equilibrium of the autonomous

Table 3.1
The existence and stability of equilibria.

Equilibrium/Bifurcation	Conditions of existence	Conditions of stability	Stability
$\mathcal{E}^0(0,0,0,0)$	Always exists	$a < -\frac{\beta_2 m}{s_1} - \frac{c\delta pm}{\mu_3 s_2 s_1}$	LAS
$\mathcal{E}^1(\frac{a}{d}, 0, 0, 0)$	$\delta \geq 0, p \geq 0, m = 0, a > 0$	$\delta \geq 0, p \geq 0, m = 0, a > 0$	LAS
$\mathcal{E}^2(\frac{a s_1 + \beta_2 m}{d s_1}, \frac{m a s_1 + \beta_2 m^2}{d s_1^2}, 0, 0)$	$\delta \geq 0, p = 0, m > 0, a > -\frac{\beta_2 m}{s_1}$	$\delta \geq 0, p = 0, m > 0, a > -\frac{\beta_2 m}{s_1}$	LAS
$\mathcal{E}^3(\frac{a s_1 + \beta_2 m}{d s_1}, \frac{m a s_1 + \beta_2 m^2}{d s_1^2}, \frac{p m a s_1 + p \beta_2 m^2}{d s_1^2 s_2}, 0)$	$\delta = 0, p > 0, m > 0, a > -\frac{\beta_2 m}{s_1}$	$\delta = 0, p > 0, m > 0, a > -\frac{\beta_2 m}{s_1}$	LAS
\mathcal{E}^* (P^*, S^*, E^*, M^*)	$\delta > 0, p > 0, m > 0, a > -\frac{\beta_2 m}{s_1} - \frac{c\delta pm}{\mu_3 s_2 s_1}$	$\delta > 0, p > 0, m > 0, a > -\frac{\beta_2 m}{s_1} - \frac{c\delta pm}{\mu_3 s_2 s_1}$	LAS
Transcritical bifurcation	$\delta \geq 0, p \geq 0, m \geq 0, a = -\frac{\beta_2 m}{s_1} - \frac{c\delta pm}{\mu_3 s_2 s_1}$	Non structurally stable	

model. As a global sensitivity analysis method, the Sobol method aims at decomposing the variance of the model output in terms of contributions of each single input parameter, or combinations thereof. Both the First-order Sobol' indices (FSI) and the Total Sobol' indices (TSI) are computed with Latin hypercube sampling (LHS) method to acquire the sensitivity characteristics (Marelli and Sudret, 2014). The default parameter value is V_0 in Table 2.1, and the parameter variation range is $\pm 10\%$ of V_0 . The number of samples is 10 000. In order to assess 95% confidence intervals (CI) for FSI and TSI, we use bootstrapping with 1000 times resampling (Efron and Tibshirani, 1994). In addition, when using the bootstrapping method, convergence can be assessed based on the width of the confidence interval. Standard Regression Coefficients (SRC) and Standard Rank Regression Coefficients (SRRC) verified the results obtained by Sobol method (Marelli et al., 2022).

2.4. Model validation

The field observations for *A. aurita* were collected in Jiaozhou Bay during the years 2009 and 2011 (Wang and Sun, 2015; Wan and Zhang, 2012). Fourier functions proved instrumental in fitting temperature trends over time (Luo, 2013; Xie et al., 2021). Parameters are adjusted based on their sensitivity, with a focus on accurately selecting sensitive parameters in alignment with empirical data while adjusting others as necessary. Through this optimization process, we fit the population sizes of all life stages and compared the fitted curves with standardized field observations and empirical findings. To delve deeper into the effects of seasonal fluctuations on *A. aurita*, an analysis of their interannual variations is performed using temperature data spanning from 2014 to 2022 in Jiaozhou Bay, XiaoMaiDao (120.4°E, 36.0°N). With climate change, the annual rise in sea surface temperatures has a significant impact on the population of *A. aurita*. Projecting forward from 2032 to 2042, temperatures are assumed to increase by an average of 0.5 °C annually with 2022 as the reference year.

3. Results

3.1. Theoretical findings

Let $a = \alpha(T(t))(1 - \kappa(T(t))) - \mu_1$, $\beta_2 = \beta_2(T(t))$, $c = \gamma\eta$, $m = \beta_1(T(t))\kappa(T(t))$, $s_1 = \beta_2(T(t)) + \mu_1$, $p = \rho(T(t))\beta_2(T(t))$, $s_2 = \delta(T(t)) + \mu_2$, $\delta = \delta(T(t))$. Then the model (2.5) becomes:

$$\begin{cases} \frac{dP}{dt} = aP + \beta_2 S + cM - dP^2, \\ \frac{dS}{dt} = mP - s_1 S, \\ \frac{dE}{dt} = pS - s_2 E, \\ \frac{dM}{dt} = \delta E - \mu_3 M, \end{cases} \quad (3.1)$$

where $\beta_2, c, d, s_1, s_2, \mu_3 > 0$, $m, p, \delta \geq 0$, $a \in \mathbb{R}$.

All theoretical findings are summarized in Table 3.1, and detailed proofs are shown in Appendix.

3.2. SAs by Sobol method and SRC method

Table 3.2 presents the FSI and TSI of polyp together with the 95% bootstrap confidence intervals. The left part of the table (columns 1 until 6) presents the results of the FSI, while the right half (columns 7 until 12) shows the TSI. Column 2 (8) shows the FSI value, as calculated with the 10 000 samples. Column 3 (9) shows the averages of the 1000 bootstrap resampling results. It may be observed that the pairwise results of columns 2 and 3 (8 and 9) are almost equal, which indicates that our bootstrapping is unbiased. The CI on the sensitivity indices are shown in columns 4 and 5 (10 and 11). The widths of the 95% CI presented in columns 6 (12) are narrow, indicating that both FSI and TSI ultimately converge. Additionally, it is noteworthy that the width of the CI for FSI is greater than that for TSI. This discrepancy may arise from FSI capturing the impact of individual input variables on the output variable, which is subject to interference from noise and other variables, resulting in a larger estimated variance and, consequently, an expanded confidence interval width. Tables 3.3-3.5 present similar results.

From Fig. 3.1(a), it can be intuitively observed that there are differences in the FSI values among the various parameters. The budding reproduction rate (α) possesses a very diminutive FSI value, and the polyp strobilation rate (κ) has a high FSI value, indicating that the contribution of asexual reproduction to the stable size of polyp lies primarily in the percentage rather than the speed of budding. The FSI value of β_2 is close to zero, suggesting that polyps are insensitive to changes in the strobila regression rate. Therefore, increasing food availability has a relatively minor impact on the relationship between strobila regression and polyp population. Parameters γ , η , and μ_3 exhibit high FSI values, indicating that a significant source of increase in polyp population comes from the sexual reproduction of medusae. The FSI value of μ_1 is low, whereas that of d is relatively high, suggesting that the polyp population is more sensitive to intraspecific competition than natural mortality or predation rates. For strobilae, the FSI values of β_1 and κ are significantly higher than that of other parameters, indicating that strobilae are most sensitive to strobilation, in alignment with real-world observations. Concerning ephyrae, the FSI values of β_1 , κ , and η are notably higher than other parameters, suggesting that ephyrae population is most sensitive to strobilation, while growth, development, and mortality of ephyrae are not as sensitive. For medusae, the FSI values of β_1 , κ , and ρ are high, indicating that bottom-up supplementation contributes significantly to the increase in stable medusa size, the high FSI value of μ_3 suggests that bottom-up supplementation contributes significantly to decreasing stable medusa size.

Regarding the parameters related to strobilation, polyp strobilation rate (β_1) and polyp strobilation proportion (κ) exhibit notably high FSI values across the four stages, the strobila development rate (β_2) demonstrate markedly low FSI values in all four stages, indicating that the initial stage of strobilation plays a critical role in influencing the population size of the Aurelia population. Medusa mortality (μ_3) plays a significant role in impeding the growth of the stable jellyfish population size, particularly influencing the equilibrium states of polyps and medusae, with lesser effects on the remaining two states. In contrast, the intraspecific competition rate (d) primarily impacts the benthic stages.

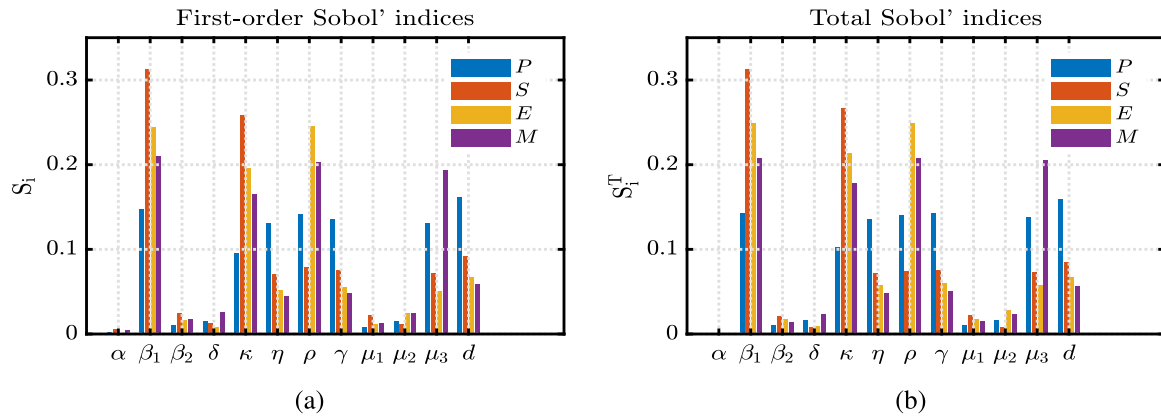


Fig. 3.1. Sobol' sensitivity results for the dependence of *A. aurita* on each parameter. (a) and (b) show the FSI and TSI of polyps, strobilae, ephyrae, and medusae, respectively.

Table 3.2

The FSI and TSI of P with bootstrap confidence intervals.

Param.	FSI value	Bootstrap average	95% CI percentile meth.		Width of 95% CI	Param.	TSI value	Bootstrap average	95% CI percentile meth.		Width of 95% CI
α	0.0058	0.0057	-0.0006	0.0121	0.0127	α	0.0006	0.0006	0.0006	0.0006	0.0000
β_1	0.1447	0.1446	0.1385	0.1507	0.0122	β_1	0.1439	0.1439	0.1454	0.1423	0.0031
β_2	0.0147	0.0146	0.0083	0.0210	0.0127	β_2	0.0095	0.0095	0.0096	0.0093	0.0003
δ	0.0204	0.0203	0.0142	0.0266	0.0124	δ	0.0155	0.0155	0.0157	0.0153	0.0004
κ	0.1043	0.1042	0.0984	0.1105	0.0121	κ	0.1030	0.1030	0.1042	0.1021	0.0021
η	0.1392	0.1391	0.1330	0.1456	0.0126	η	0.1373	0.1373	0.1387	0.1361	0.0026
ρ	0.1392	0.1390	0.1331	0.1452	0.0121	ρ	0.1372	0.1371	0.1384	0.1358	0.0026
γ	0.1403	0.1402	0.1342	0.1460	0.0118	γ	0.1385	0.1385	0.1400	0.1370	0.0030
μ_1	0.0152	0.0151	0.0089	0.0213	0.0124	μ_1	0.0103	0.0103	0.0104	0.0102	0.0002
μ_2	0.0212	0.0211	0.0150	0.0271	0.0121	μ_2	0.0154	0.0154	0.0155	0.0152	0.0003
μ_3	0.1388	0.1388	0.1327	0.1447	0.0120	μ_3	0.1384	0.1384	0.1396	0.1370	0.0026
d	0.1618	0.1618	0.1558	0.1679	0.0121	d	0.1603	0.1603	0.1621	0.1583	0.0038

Table 3.3

The FSI and TSI of S with bootstrap confidence intervals.

Param.	FSI value	Bootstrap average	95% CI percentile meth.		Width of 95% CI	Param.	TSI value	Bootstrap average	95% CI percentile meth.		Width of 95% CI
α	0.0039	0.0038	-0.0024	0.0100	0.0124	α	0.0003	0.0003	0.0003	0.0003	0.0000
β_1	0.3074	0.3072	0.3015	0.3127	0.0112	β_1	0.3158	0.3158	0.3125	0.3187	0.0062
β_2	0.0240	0.0239	0.0177	0.0302	0.0125	β_2	0.0210	0.0210	0.0207	0.0213	0.0006
δ	0.0116	0.0114	0.0052	0.0178	0.0126	δ	0.0082	0.0082	0.0081	0.0083	0.0002
κ	0.2621	0.2620	0.2562	0.2677	0.0115	κ	0.2694	0.2695	0.2671	0.2723	0.0052
η	0.0737	0.0735	0.0673	0.0796	0.0123	η	0.0727	0.0727	0.0721	0.0734	0.0013
ρ	0.0724	0.0722	0.0663	0.0786	0.0123	ρ	0.0726	0.0725	0.0718	0.0732	0.0014
γ	0.0732	0.0730	0.0668	0.0794	0.0126	γ	0.0734	0.0734	0.0726	0.0741	0.0015
μ_1	0.0249	0.0248	0.0186	0.0310	0.0124	μ_1	0.0221	0.0221	0.0218	0.0223	0.0005
μ_2	0.0121	0.0120	0.0057	0.0183	0.0126	μ_2	0.0081	0.0081	0.0080	0.0082	0.0002
μ_3	0.0717	0.0716	0.0654	0.0777	0.0123	μ_3	0.0733	0.0733	0.0726	0.0740	0.0014
d	0.0842	0.0842	0.0778	0.0905	0.0127	d	0.0847	0.0846	0.0835	0.0856	0.0021

Table 3.4

The FSI and TSI of E with bootstrap confidence intervals.

Param.	FSI value	Bootstrap average	95% CI percentile meth.		Width of 95% CI	Param.	TSI value	Bootstrap average	95% CI percentile meth.		Width of 95% CI
α	0.0032	0.0031	-0.0032	0.0098	0.0130	α	0.0002	0.0002	0.0002	0.0003	0.0001
β_1	0.2418	0.2416	0.2357	0.2477	0.0120	β_1	0.2519	0.2519	0.2492	0.2549	0.0057
β_2	0.0188	0.0187	0.0122	0.0257	0.0135	β_2	0.0167	0.0167	0.0165	0.0169	0.0004
δ	0.0109	0.0108	0.0046	0.0173	0.0127	δ	0.0086	0.0086	0.0085	0.0087	0.0002
κ	0.2066	0.2066	0.2004	0.2126	0.0122	κ	0.2148	0.2148	0.2126	0.2176	0.0050
η	0.058	0.0578	0.0516	0.0642	0.0126	η	0.058	0.058	0.0574	0.0585	0.0011
ρ	0.2366	0.2365	0.2308	0.2424	0.0116	ρ	0.2446	0.2444	0.2423	0.2468	0.0045
γ	0.0584	0.0583	0.0521	0.0645	0.0124	γ	0.0586	0.0586	0.0579	0.0592	0.0013
μ_1	0.0195	0.0194	0.0130	0.0258	0.0128	μ_1	0.0174	0.0174	0.0173	0.0176	0.0003
μ_2	0.0308	0.0307	0.0245	0.0373	0.0128	μ_2	0.0279	0.0279	0.0276	0.0282	0.0006
μ_3	0.0572	0.0571	0.0511	0.0634	0.0123	μ_3	0.0586	0.0585	0.0579	0.0591	0.0012
d	0.0673	0.0672	0.0608	0.0740	0.0132	d	0.0675	0.0675	0.0666	0.0682	0.0016

Parameter interactions have the potential to introduce deviations in outcomes and diminish the precision of sensitivity analyses. The

Total Sensitivity Indices (TSIs) play a crucial role in delineating parameter interactions. Fig. 3.1(b) exhibits a distribution akin to that

Table 3.5
The FSI and TSI of M with bootstrap confidence intervals.

Param.	FSI value	Bootstrap average	95% CI percentile meth.	Width of 95% CI	Param.	TSI value	Bootstrap average	95% CI percentile meth.	Width of 95% CI
α	0.0039	0.0038	-0.0024	0.0100	α	0.0002	0.0002	0.0002	0.0002
β_1	0.2000	0.1999	0.1942	0.2058	β_1	0.2099	0.2099	0.2076	0.2123
β_2	0.0168	0.0167	0.0102	0.0232	β_2	0.0140	0.0139	0.0138	0.0141
δ	0.0255	0.0253	0.0190	0.0319	δ	0.0232	0.0232	0.0230	0.0235
κ	0.1724	0.1723	0.1660	0.1785	κ	0.1792	0.1793	0.1773	0.1813
η	0.0487	0.0485	0.0422	0.0548	η	0.0483	0.0483	0.0478	0.0488
ρ	0.1962	0.1960	0.1899	0.2020	ρ	0.2035	0.2033	0.2018	0.2052
γ	0.0494	0.0493	0.0432	0.0554	γ	0.0488	0.0488	0.0482	0.0493
μ_1	0.0175	0.0174	0.0111	0.0238	μ_1	0.0145	0.0145	0.0143	0.0147
μ_2	0.0265	0.0263	0.0203	0.0328	μ_2	0.0230	0.0230	0.0228	0.0233
μ_3	0.1979	0.1978	0.1918	0.2035	μ_3	0.2072	0.2072	0.2053	0.2091
d	0.0564	0.0563	0.0499	0.0629	d	0.0562	0.0562	0.0555	0.0569

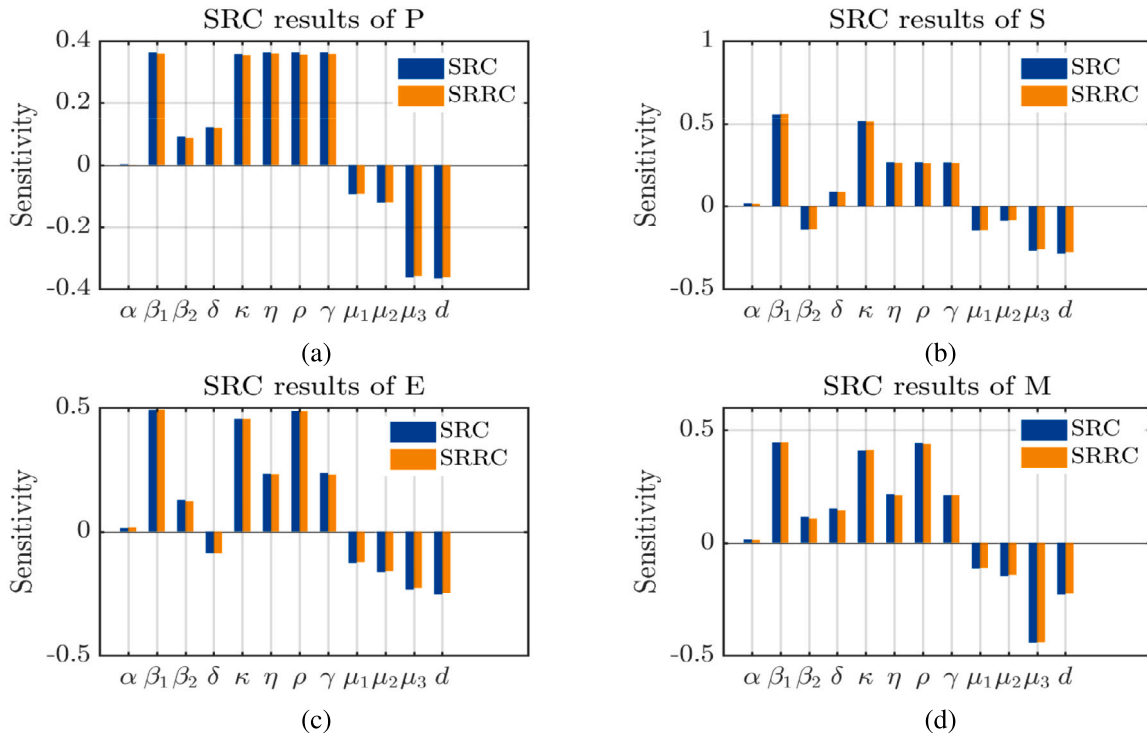


Fig. 3.2. SRC and SRRC sensitivity results. (a)–(d) show the SRC and SRRC indices of polyps, strobilae, ephyrae, and medusae, respectively.

of Fig. 3.1(a), indicating that parameter interactions have a minor impact on sensitivity analysis results. By screening these parameters, optimization efficiency can be enhanced, leading to more rational predictions.

3.3. Model validation and application

Fig. 3.3 illustrates the long-term periodic variations in sea surface temperature (SST) within Jiaozhou Bay from 2009 to 2022. Annual temperature variations follow consistent trends, with peak and nadir values typically observed in August and February, respectively.

We substitute the fitting functions for temperature-influenced parameters (i.e., α , β_1 , β_2 , δ , ρ , κ) into the model to conduct analysis. *Aurelia* sp. strobilation in temperate regions optimally occurs between 13 °C to 15 °C, offering two yearly opportunities aligned with temperature changes from late summer to autumn and from winter to early spring (Chi et al., 2022; Lucas et al., 2012). The experiment conducted by Chi et al. implies that strobilation rates (%) of the second strobilation process is five times that of the first (Chi et al., 2022). It also indicates that, strobilation of polyps commenced 3 weeks subsequent to the temperature declining to 13 °C prior to overwintering, and 2 weeks

following the temperature rising to 13 °C after the overwintering phase (Chi et al., 2022). Therefore, we adjust $\kappa(t)$ and $\beta_1(t)$ to one-fifth and two-third of their original values for the autumn and winter periods, respectively.

With the increase of temperature, on the one hand, the natural mortality rate of ephyrae decreases (Duan et al., 2020), on the other hand, the number of ephyrae predators such as fishes and other zooplankton also increases (Kogovšek et al., 2012), so we assume that the mortality rate of ephyrae μ_2 remains unchanged during this stage. Until the temperature rises to a certain extent, the activity of ephyrae drops dramatically and the population rapidly decreases (Yu et al., 2023). Therefore, $\mu_2(T)$ is defined as

$$\mu_2(T) = \begin{cases} 0.05, & T < 21, \\ 0.09, & T > 21. \end{cases}$$

Similarly, medusae’s mortality is affected by temperature, food, and other biological factors (Kogovšek et al., 2012). During the transition from ephyrae to medusae, favorable conditions such as optimal temperature and ample food facilitate rapid growth with low mortality rates (Zheng et al., 2010). However, during summer and autumn, medusae activity declines sharply as planulae are released (Lucas,

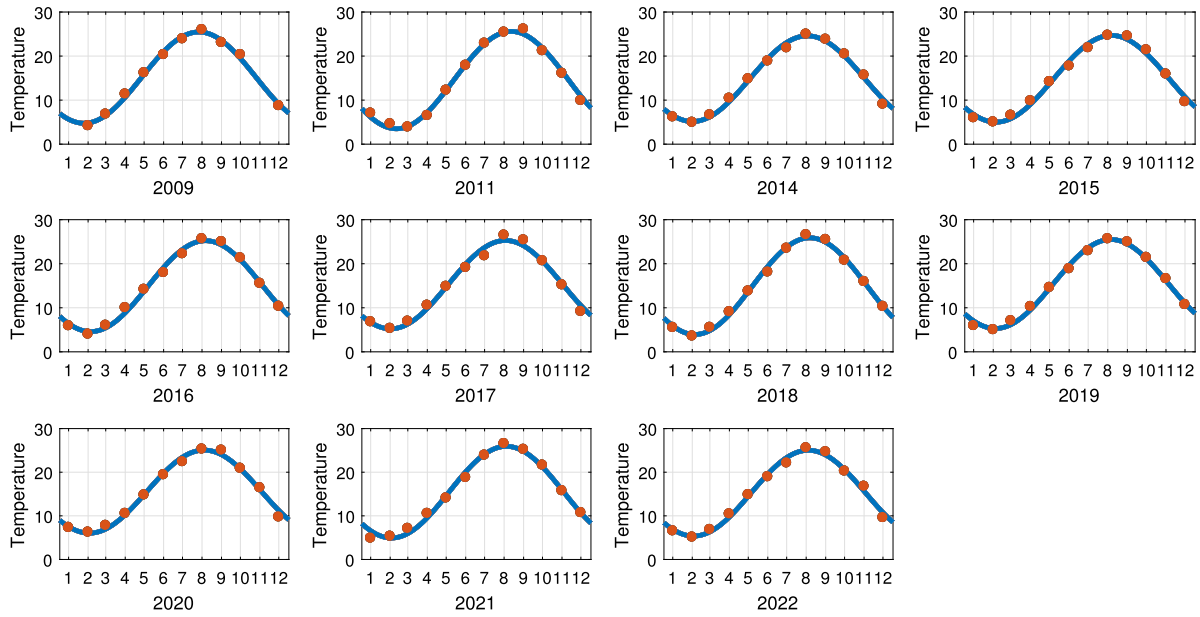


Fig. 3.3. Sea surface temperature in Jiaozhou Bay from 2009 to 2022. The blue curves represent the fitted temperature trends over time, while the solid orange circles denote the empirical monthly mean sea surface temperature data.

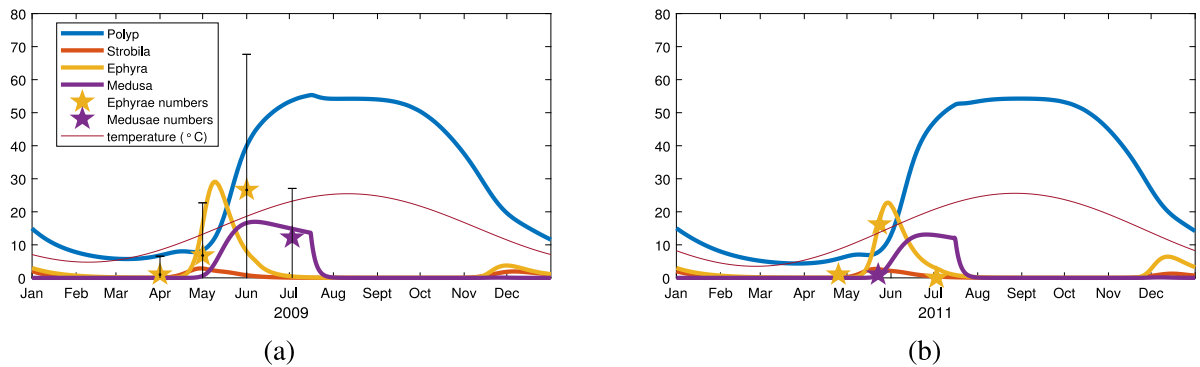


Fig. 3.4. Fitted populations of *A. aurita* in Jiaozhou Bay during 2009 and 2011. Errorbars represent standard deviation.

2001; Wang and Sun, 2015). Moreover, the high temperatures reduce the zooplankton population, failing to meet the energy needs of the medusae, leading to a rapid decline in their numbers during this period (Yu et al., 2023). Thus, we define $\mu_3(t)$ as

$$\mu_3(t) = \begin{cases} 0.0065, & 1 \leq t < 196, \\ 0.3, & 196 \leq t \leq 366. \end{cases}$$

The remaining parameters share the same value with V_0 in Table 2.1. And we set the initial value as (15, 2, 3, 0). Fig. 3.4(a) and (b) illustrate the fluctuation patterns of four life stages of *A. aurita* in 2009 and in 2011. Polyps were consistently present throughout the year, exhibiting trends closely mirroring those of temperature changes, except in April. The fitted curve for polyps in April displayed a bell-shaped pattern, suggesting a significant number of polyps are undergoing strobilation to develop into strobilae. Subsequently, from May to July, the polyp population rapidly increased, peaking in July. This surge can be attributed to the favorable temperature conditions for polyp budding reproduction during this period, coupled with the release of a large number of planulae by mature medusae, which metamorphose into polyps. In comparison to 2009, strobilation occurred later in 2011, resulting in delayed appearances of ephyrae and medusae, with reduced numbers. This could be attributed to the lower average temperatures and slower temperature increase during the spring of 2011, which are unfavorable for strobilation.

Both strobilae and ephyrae exhibit biannual fluctuations before and after overwintering. The strobilation process in late autumn is not as pronounced as that in spring, a result that appears to support the findings of Chi et al. (2022). Medusae only appears in spring and summer, with ephyrae observed in December failing to mature into medusae. The medusae population experiences a rapid increase in May, maintaining a relatively high level in June and July before sharply declining. Field observations closely align with the fitted results within the margin of error, indicating the efficacy of the hypothesis, affirming the model's rationality, and validating the accuracy of parameter fitting.

3.4. Predictions under climate change

In the context of climate change, the annual rise in sea surface temperatures has a significant impact on the population of *A. aurita*. From 2014 to 2022, we utilized the temperatures fitting data provided in Fig. 3.3. The population of *A. aurita* experienced fluctuations with an approximate periodicity from 2014 to 2022 in response to seasonal variations (see Fig. 3.5). These fluctuations mirrored those observed in 2009 and 2011. Fig. 3.5 indicates that this temperature increase noticeably affects the numbers of strobila, ephyrae, and medusae, exhibiting a trend of initial increase followed by a decrease. This pattern seems to reflect the fact that while elevated temperatures initially enhance

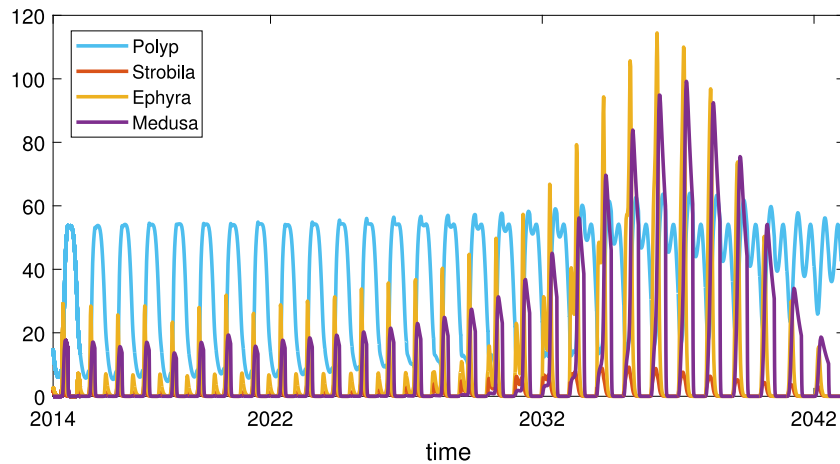


Fig. 3.5. Populations of *A. aurita* in Jiaozhou Bay from 2014 to 2042.

the growth and reproduction of *A. aurita*, there are limits to this stimulation, and excessively high temperatures may actually suppress their growth and reproduction. Conversely, the benthic polyp stage appears less affected by temperature. This might suggest that this physiological characteristic enables the *A. aurita* species to persist. When external conditions become favorable, they can regenerate medusae, potentially leading to jellyfish bloom phenomena.

Since we have separately represented the strobila stage (S) in our model (2.5), the process of strobila regression into the benthic polyp stage (P) can be clearly expressed. Therefore, the impact of strobila regression and subsequent strobilation on the population of upper-level planktonic medusae in seawater can be explored. As shown in Fig. 3.6, the yellow curve depicts the ephyrae undergoing regression process, while the pink curve represents ephyrae without regression process. It can be observed that as the number of ephyrae increases with rising temperatures, the increase in the number of ephyrae due to degeneration also intensifies. However, as the temperature continues to rise, this gain diminishes rapidly. By 2041, the number of disk-shaped medusae is close to the numbers observed from 2014 to 2022. Interestingly, the yellow and pink curves almost overlap in 2041, indicating that the process of strobila degeneration has no significant promoting effect on the production of disk-shaped medusae. Similarly, the regression process also exhibits similar effects on the medusa stage (see Fig. 3.7).

3.5. Control recommendation

Due to the detrimental effects of jellyfish outbreaks, there is significant interest in whether jellyfish will proliferate and to what extent. Introducing strobilae into model (2.5) offers new insights into predicting jellyfish outbreaks. As shown in Fig. 3.8, the strobilation process began earliest in 2020 and latest in 2018. This appears to result in ephyrae occurring earliest in 2020 and latest in 2018 (see Fig. 3.9). Reflected in the maximum population numbers of medusa, the peak in 2020 far exceeds that in 2018 (see Fig. 3.10). It may suggest that earlier strobilation gives *A. aurita* a competitive advantage in ecosystems, potentially leading to summer *A. aurita* outbreaks. Ephyrae population size can be surveyed in April and May, and if it exceeds a certain threshold, early warnings can be activated to initiate preventive or responsive measures against *A. aurita* outbreaks.

While increasing μ_3 appears to be the most direct and effective method for controlling the number of medusae based on Fig. 3.2 (d), this approach is not practical due to (1) the potential ecological and socio-economic harm already caused by a large population of medusae at that point, and (2) the labor-intensive and resource-demanding nature of killing mature medusae, which can also stimulate jellyfish

reproduction through the release of large quantities of sperm and eggs upon damage (Uye and Shimauchi, 2005; Yu et al., 2023). Hence, it is advisable to control their population during the early stages of jellyfish development. Specifically, this involves restricting substrate expansion during the benthic phase, increasing ephyrae mortality rates during the planktonic phase, and reducing the survival rate of newly produced planulae. Fig. 3.11(a)–(c) illustrates these findings, showing that medusae persist at small scales when both d and μ_2 increase, but face extinction when γ decreases. Fig. 3.11(d)–(f) show the number of medusae over time with different values of μ_2 , d and γ , respectively. Fig. 3.12 displays the control efficiencies with varying parameters, suggesting that under sustained lower γ levels, an accelerated acquisition of small-scale medusae may occur with increasing d and μ_2 .

4. Discussion

A four-stage (Polyp–Strobila–Ephyra–Medusa) life cycle model of *A. aurita* is formulated to elucidate the influence of temperature and seasonal changes on population dynamics. Numerical simulations provided evidence that the presence of medusae was contingent upon the incidence of strobilation and the development of ephyrae. Regression and subsequent strobilation favor an increase in the pelagic medusae population. In addition, the influence of climate change on the growth and reproduction of *A. aurita* shows initial stimulation followed by inhibition. Moreover, earlier strobilation in spring may lead to more extensive medusae outbreaks in summer, providing insights for early warning of jellyfish blooms.

Compared to the MPE system described in Yu et al. (2023), the PSEM system established in this paper places greater emphasis on the strobila stage. We investigated how the duration of strobilation period influences the medusae population, reflected through changes in β_2 . β_2 represents the reciprocal sum of the bet-strobilation and strobilation period; assuming the strobilation period is four times the bet-strobilation, $5\beta_2$ indicates no strobilation period. As depicted in Fig. 4.1, an increase in β_2 corresponds to a higher medusa population. We speculate that failing to account for the strobilation period could lead to overestimating predicted jellyfish numbers. Our conclusions share some similarities with those of Yu et al. (2023) but differ in the primary timing of strobilation, which predominantly takes place in spring rather than autumn in our study. In fact, after experiencing extremely low temperatures during the overwintering period, the preparation time for strobilation in spring is shortened, and the proportion of individuals engaging in strobilation is increased (Zang et al., 2022). The results of numerical simulations align with the conclusions in Chi et al. (2022), which state that strobilation following overwintering is the primary process for planktonic medusae recruitment in temperate regions. Indeed, due to

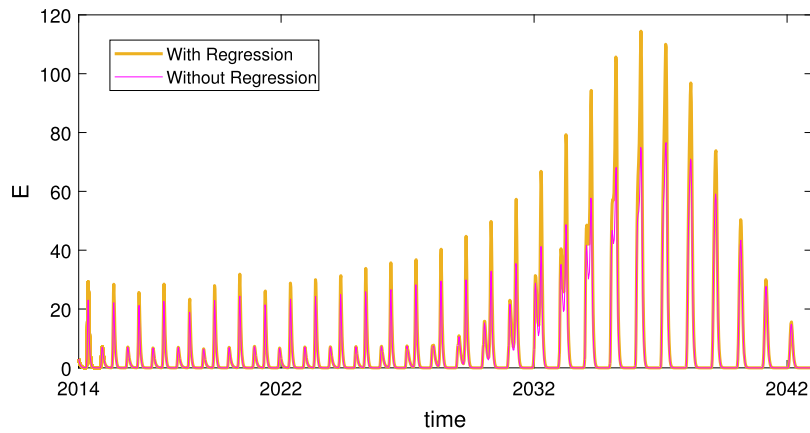


Fig. 3.6. Population forecasting of ephyrae under climate change.

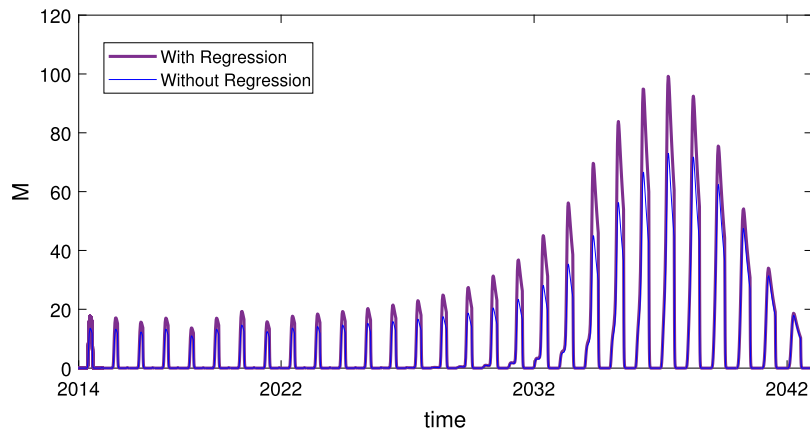


Fig. 3.7. Population forecasting of medusae under climate change.

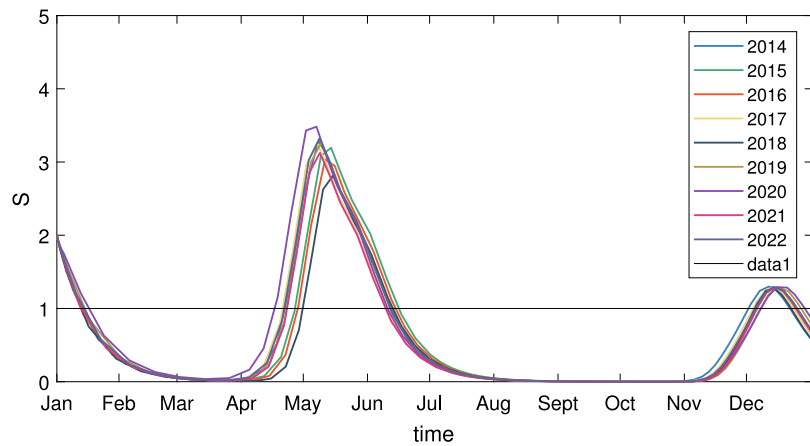


Fig. 3.8. Fitted population size of the strobila stage of *A. aurita* in Jiaozhou Bay from 2014 to 2022.

the wide distribution of *Aurelia* spp., the strobilation of polyps may exhibit site-specific patterns, as highlighted in Lucas et al. (2012). For instance, in Gullmar Fjord and Thau Lagoon, it was observed that the strobilation rate in November was significantly higher than that from February to April (Marques et al., 2019; Hernroth and Gröndahl, 1985). By calibrating the relevant parameters based on actual data, our model may have a wider range of applications.

SAs outcomes validated that the population sizes of medusae are predominantly influenced by bottom-up enrichment, highlighting strobilation as the primary mechanism propelling *A. aurita* proliferations. Parameters associated with strobilation are significantly influenced by

temperature, suggesting a close relationship between the density of planktonic *A. aurita* populations and temperature. In the last 40 years, seasonal water temperatures in Jiaozhou Bay have increased, particularly during winter (Sun et al., 2011; Zang et al., 2022). These changes are likely favorable for the growth and reproduction of jellyfish in Jiaozhou Bay, leading to jellyfish outbreaks.

Furthermore, polyp competition (d), sexual reproduction (η and γ), ephyrae mortality (μ_2), and medusae mortality (μ_3) play pivotal roles, with a relatively minor influence observed from asexual reproduction. This implies that reducing substrates and fishing pressure on ephyrae-consuming fish can help prevent rapid increases in jellyfish numbers

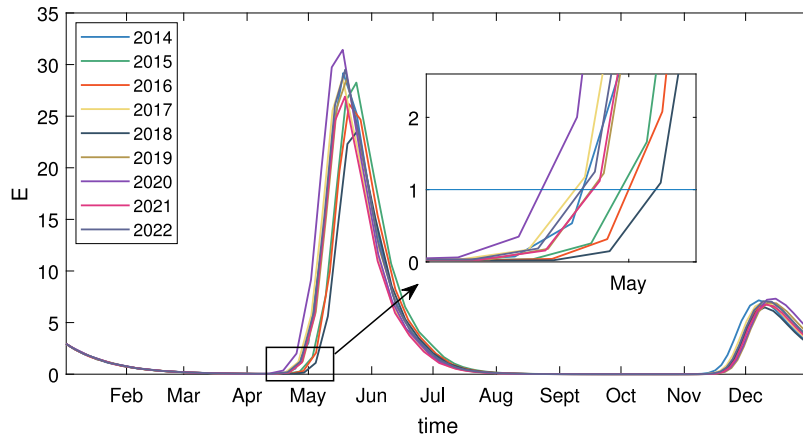


Fig. 3.9. Fitted population size of the ephyra stage of *A. aurita* in Jiaozhou Bay from 2014 to 2022.

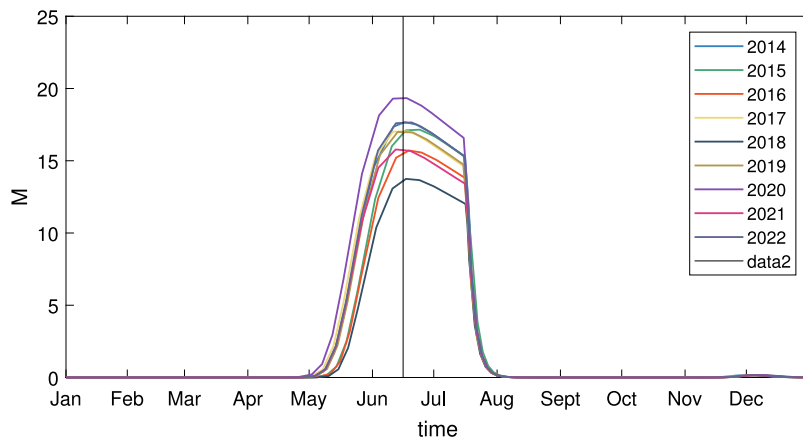


Fig. 3.10. Fitted population size of the medusa stage of *A. aurita* in Jiaozhou Bay from 2014 to 2022.

and subsequent bloom formation in early spring. Since planulae tend to settle on artificial substrates such as bricks, ropes, cans, wood, concrete, plastic, and glass (Duarte et al., 2013), coastal managers should consider modifying the design and surface characteristics of artificial structures deployed in the coastal zone and regulate waste disposal to avoid introducing substrates like plastics.

Our current research exhibits certain constraints necessitating further investigation. From a pragmatic perspective, a direct link can be established between the utilized parameters and the genuine population responses, achievable through an optimized model. Additionally, our focus has been exclusively on the intricate life history of the population, overlooking its ecological role. An ecosystem functions as a unified and interconnected entity where modifications in both biotic and abiotic elements hold the potential to influence the *A. aurita* population. Subsequent studies could integrate a wider array of environmental factors, including light intensity, salinity, and diverse biological communities like fish, planktonic organisms, and biofouling species, into the model, highlighting the unique attributes of *A. aurita* as a keystone species.

CRedit authorship contribution statement

Wei Wang: Writing – review & editing, Supervision, Methodology, Funding acquisition, Data curation, Conceptualization. **Mengjie Wang:** Writing – original draft, Visualization, Software, Methodology, Investigation, Formal analysis. **Hao Wang:** Writing – review & editing, Validation, Project administration, Investigation, Conceptualization.

Declaration of competing interest

The authors declare that they have no known competing financial interests or personal relationships that could have appeared to influence the work reported in this paper.

Acknowledgments

We thank the anonymous referee and the handling editor for their valuable comments which have led to a substantial improvement in the revision. Wei Wang gratefully acknowledges support from the National Natural Science Foundation of China (No. 12271308, 11901360). Hao Wang gratefully acknowledges support from the Natural Sciences and Engineering Research Council of Canada, Canada (Discovery Grant RGPIN-2020-03911 and Accelerator Grant RGPAS-2020-00090) and the CRC program (Tier 1 Canada Research Chair Award).

Appendix

Theorem A.1. *The extinction equilibrium $\mathcal{E}^0(0, 0, 0, 0)$ of model (3.1) always exists. If $a < -\frac{\beta_2 m}{s_1} - \frac{c \delta p m}{\mu_3 s_2 s_1}$, then \mathcal{E}^0 is locally asymptotically stable (LAS); if $a = -\frac{\beta_2 m}{s_1} - \frac{c \delta p m}{\mu_3 s_2 s_1}$, then \mathcal{E}^0 is stable but not asymptotically stable; if $a > -\frac{\beta_2 m}{s_1} - \frac{c \delta p m}{\mu_3 s_2 s_1}$, then \mathcal{E}^0 is unstable.*

Proof. The existence of \mathcal{E}^0 is trivially verified. The Jacobian matrix of (3.1) at \mathcal{E}^0 is

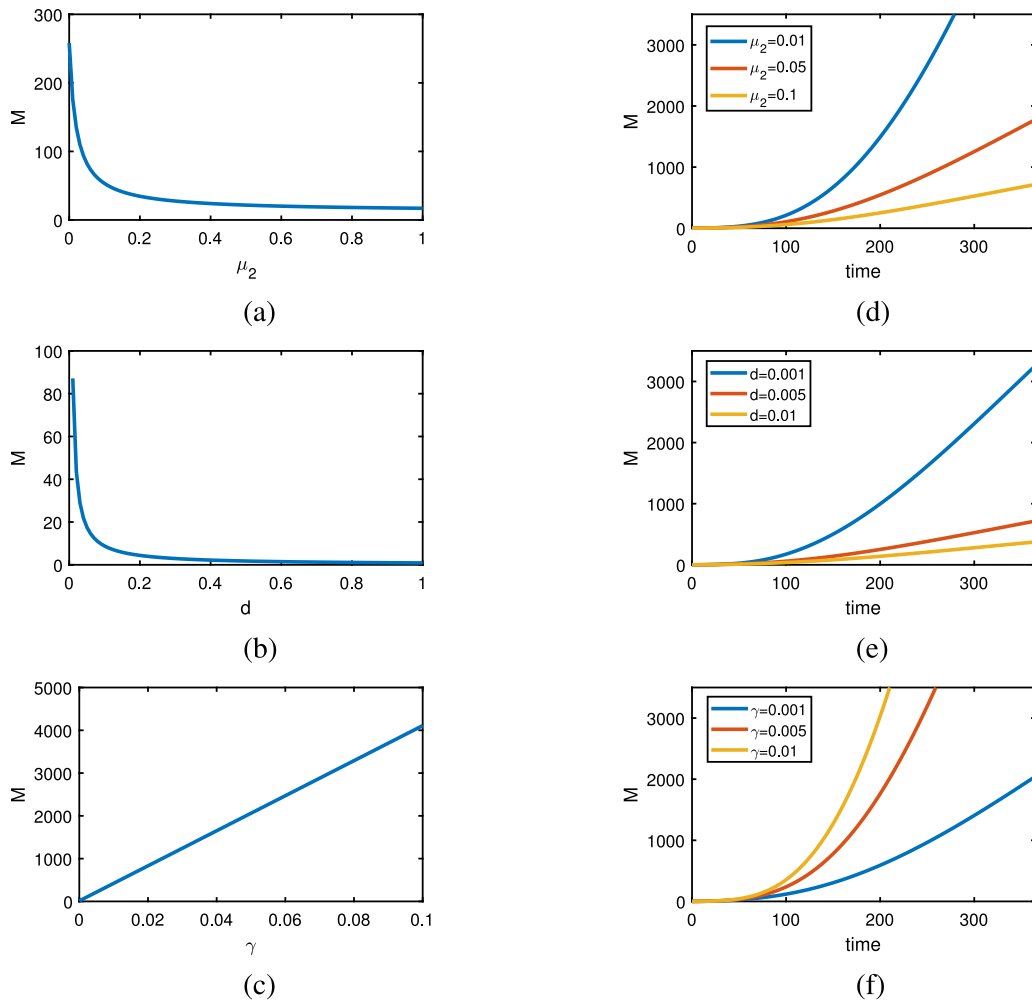


Fig. 3.11. Control strategies for model (2.5). (a)–(c) are medusae changing with μ_2 , d , γ , respectively. (d)–(e) are medusae changes with time under different values of μ_2 , d , γ , respectively. All the other values of parameters take V_0 in Table 2.1.

$$J(\mathcal{E}^0) = \begin{pmatrix} -v & \beta_2 & 0 & c \\ m & -s_1 & 0 & 0 \\ 0 & p & -s_2 & 0 \\ 0 & 0 & \delta & -\mu_3 \end{pmatrix},$$

where $v = -a$. Then the characteristic equation is

$$\lambda^4 + (\mu_3 + s_2 + s_1 + v)\lambda^3 + [\mu_3 s_2 + (s_1 + v)(\mu_3 + s_2) + s_1 v - m\beta_2]\lambda^2 + [(s_1 + v)\mu_3 s_2 + (s_1 v - m\beta_2)(s_2 + \mu_3)]\lambda + (s_1 v - m\beta_2)\mu_3 s_2 - mcp\delta = 0.$$

Then we have

$$\Delta_1 = \mu_3 + s_2 + s_1 + v,$$

$$\Delta_2 = (\mu_3 + s_2)\mu_3 s_2 + (\mu_3 + s_2 + s_1 + v)(s_1 + v)(\mu_3 + s_2) + (s_1 + v)(s_1 v - m\beta_2),$$

$$\begin{aligned} \Delta_3 = & (s_1 + v)(\mu_3 + s_2)\mu_3^2 s_2^2 + (\mu_3 + s_2 + s_1 + v)(s_1 + v)^2 (\mu_3 + s_2)\mu_3 s_2 \\ & + (s_1 v - m\beta_2)(s_1 + v)(\mu_3 + s_2)(\mu_3^2 + s_2^2 + (s_1 + v)(\mu_3 + s_2)) \\ & + (s_1 v - m\beta_2)^2 (s_1 + v)(\mu_3 + s_2) \\ & + mcp\delta(\mu_3 + s_2 + s_1 + v)^2, \end{aligned}$$

$$\Delta_4 = ((s_1 v - m\beta_2)\mu_3 s_2 - mcp\delta)\Delta_3.$$

By the Routh–Hurwitz criteria, if $a < -\frac{\beta_2 m}{s_1} - \frac{c\delta pm}{\mu_3 s_2 s_1}$, then \mathcal{E}^0 is LAS; if $a = -\frac{\beta_2 m}{s_1} - \frac{c\delta pm}{\mu_3 s_2 s_1}$, then \mathcal{E}^0 is stable but not asymptotically stable; if $a > -\frac{\beta_2 m}{s_1} - \frac{c\delta pm}{\mu_3 s_2 s_1}$, then \mathcal{E}^0 is unstable. ■

Theorem A.2. If $\delta \geq 0, p \geq 0, m = 0, a > 0$, then the boundary equilibrium $\mathcal{E}^1 \left(\frac{a}{d}, 0, 0, 0 \right)$ of model (3.1) exists and is LAS.

Proof. If $\delta \geq 0, p \geq 0, m = 0, a > 0$, then the existence of \mathcal{E}^1 is trivially verified. The characteristic equation for the Jacobian matrix of \mathcal{E}^1 is $\lambda^4 + (\mu_3 + s_2 + s_1 + a)\lambda^3 + [\mu_3 s_2 + (s_1 + a)(\mu_3 + s_2) + s_1 a]\lambda^2 + [s_1 + a\mu_3 s_2 + s_1 a(s_2 + \mu_3)]\lambda + s_1 a\mu_3 s_2 = 0$.

Then we have

$$\Delta_1 = \mu_3 + s_2 + s_1 + a > 0,$$

$$\Delta_2 = (\mu_3 + s_2)\mu_3 s_2 + (\mu_3 + s_2 + s_1 + a)(s_1 + a)(\mu_3 + s_2) + (s_1 + a)s_1 a > 0,$$

$$\begin{aligned} \Delta_3 = & (s_1 + a)(\mu_3 + s_2)\mu_3^2 s_2^2 + (\mu_3 + s_2 + s_1 + a)(s_1 + a)^2 (\mu_3 + s_2)\mu_3 s_2 \\ & + s_1 a(s_1 + a)(\mu_3 + s_2)(\mu_3^2 + s_2^2 + (s_1 + a)(\mu_3 + s_2)) \\ & + (s_1 a)^2 (s_1 + a)(\mu_3 + s_2) > 0, \end{aligned}$$

$$\Delta_4 = s_1 a\mu_3 s_2 \Delta_3 > 0.$$

By the Routh–Hurwitz criteria, $\mathcal{E}^1 \left(\frac{a}{d}, 0, 0, 0 \right)$ is LAS. ■

Theorem A.3. If $\delta \geq 0, p = 0, m > 0, a > -\frac{\beta_2 m}{s_1}$, then the boundary equilibrium $\mathcal{E}^2 \left(\frac{as_1 + \beta_2 m}{ds_1}, \frac{mas_1 + \beta_2 m^2}{ds_1^2}, 0, 0 \right)$ of model (3.1) exists and is LAS.

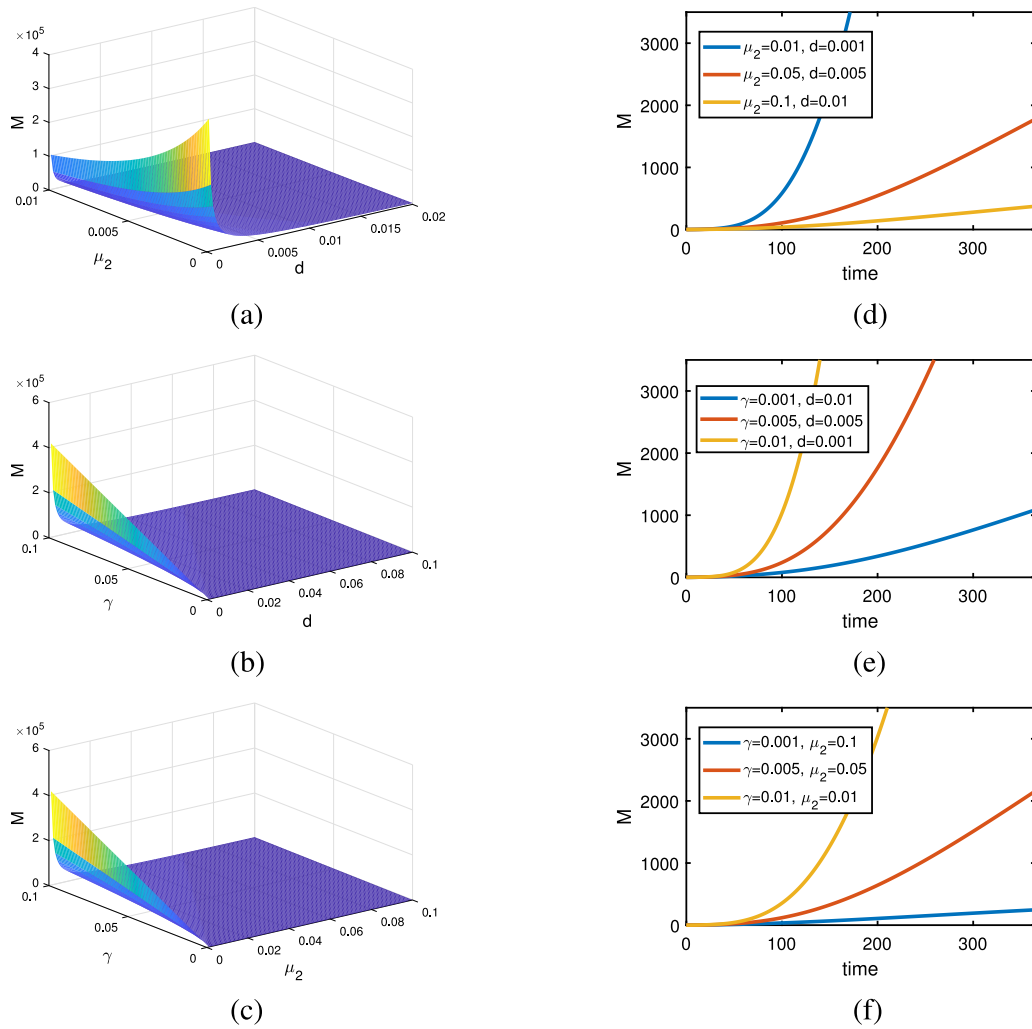


Fig. 3.12. Control strategies for model (2.5). (a)–(c) are medusae changing with μ_2 & d , γ & d , γ & μ_2 , respectively. (d)–(e) are medusae changes with time under different values of μ_2 & d , γ & d , γ & μ_2 , respectively. All the other values of parameters take V_0 in Table 2.1.

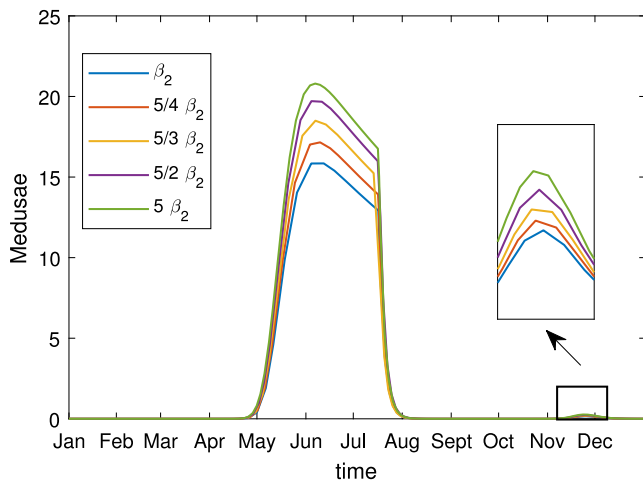


Fig. 4.1. The impact of strobilation period on medusae population.

Proof. If $\delta \geq 0, p = 0, m > 0, a > -\frac{\beta_2 m}{s_1}$, then the existence of \mathcal{E}^2 is readily verified. The characteristic equation is

$$\lambda^4 + (\mu_3 + s_2 + s_1 + v_1)\lambda^3 + [\mu_3 s_2 + (s_1 + v_1)(\mu_3 + s_2) + s_1 v_1 - m\beta_2]\lambda^2 + [(s_1 + v_1)\mu_3 s_2 + (s_1 v_1 - m\beta_2)(s_2 + \mu_3)]\lambda + (s_1 v_1 - m\beta_2)\mu_3 s_2 = 0,$$

where $v_1 = a + \frac{2\beta_2 m}{s_1} > \frac{\beta_2 m}{s_1}$. Then we have

$$\Delta_1 = \mu_3 + s_2 + s_1 + v_1 > 0,$$

$$\Delta_2 = (\mu_3 + s_2)\mu_3 s_2 + (\mu_3 + s_2 + s_1 + v_1)(s_1 + v_1)(\mu_3 + s_2) + (s_1 + v_1)(s_1 v_1 - m\beta_2) > 0,$$

$$\Delta_3 = (s_1 + v_1)(\mu_3 + s_2)\mu_3^2 s_2^2 + (\mu_3 + s_2 + s_1 + v_1)(s_1 + v_1)^2 (\mu_3 + s_2)\mu_3 s_2 + (s_1 v_1 - m\beta_2)(s_1 + v_1)(\mu_3 + s_2)(\mu_3^2 + s_2^2 + (s_1 + v_1)(\mu_3 + s_2)) + (s_1 v_1 - m\beta_2)^2 (s_1 + v_1)(\mu_3 + s_2) > 0,$$

$$\Delta_4 = (s_1 v_1 - m\beta_2)\mu_3 s_2 \Delta_3 > 0.$$

By the Routh–Hurwitz criteria, $\mathcal{E}^2(\frac{a s_1 + \beta_2 m}{d s_1}, \frac{m a s_1 + \beta_2 m^2}{d s_1^2}, 0, 0)$ is LAS. ■

Theorem A.4. If $\delta = 0, p > 0, m > 0, a > -\frac{\beta_2 m}{s_1}$, then the boundary equilibrium $\mathcal{E}^3(\frac{a s_1 + \beta_2 m}{d s_1}, \frac{m a s_1 + \beta_2 m^2}{d s_1^2}, \frac{p m a s_1 + \beta_2 m^2}{d s_1^2 s_2}, 0)$ of model (3.1) exists and is LAS.

Proof. If $\delta = 0, p > 0, m > 0, a > -\frac{\beta_2 m}{s_1}$, then the existence of \mathcal{E}^3 is readily verified. The characteristic equation is

$$\lambda^4 + (\mu_3 + s_2 + s_1 + v_2)\lambda^3 + [\mu_3 s_2 + (s_1 + v_2)(\mu_3 + s_2) + s_1 v_2 - m\beta_2]\lambda^2 + [(s_1 + v_2)\mu_3 s_2 + (s_1 v_2 - m\beta_2)(s_2 + \mu_3)]\lambda + (s_1 v_2 - m\beta_2)\mu_3 s_2 = 0,$$

where $v_2 = a + \frac{2\beta_2 m}{s_1} > \frac{\beta_2 m}{s_1}$. Then we have

$$\begin{aligned} \Delta_1 &= \mu_3 + s_2 + s_1 + v_2 > 0, \\ \Delta_2 &= (\mu_3 + s_2)\mu_3s_2 + (\mu_3 + s_2 + s_1 + v_2)(s_1 + v_2)(\mu_3 + s_2) \\ &\quad + (s_1 + v_2)(s_1v_2 - m\beta_2) > 0, \\ \Delta_3 &= (s_1 + v_2)(\mu_3 + s_2)\mu_3^2s_2^2 + (\mu_3 + s_2 + s_1 + v_2)(s_1 + v_2)^2(\mu_3 + s_2)\mu_3s_2 \\ &\quad + (s_1v_2 - m\beta_2)(s_1 + v_2)(\mu_3 + s_2)(\mu_3^2 + s_2^2 + (s_1 + v_2)(\mu_3 + s_2)) \\ &\quad + (s_1v_2 - m\beta_2)^2(s_1 + v_2)(\mu_3 + s_2) > 0, \\ \Delta_4 &= (s_1v_2 - m\beta_2)\mu_3s_2\Delta_3 > 0. \end{aligned}$$

By the Routh–Hurwitz criteria, $\mathcal{E}^3(\frac{as_1+\beta_2m}{ds_1}, \frac{mas_1+\beta_2m^2}{ds_1^2}, \frac{pmas_1+p\beta_2m^2}{ds_1^2s_2}, 0)$ is LAS. ■

Theorem A.5. If $\delta > 0, p > 0, m > 0, a > -\frac{\beta_2m}{s_1} - \frac{c\delta pm}{\mu_3s_2s_1}$, then the internal equilibrium \mathcal{E}^* (P^*, S^*, E^*, M^*) of model (3.1) exists and is LAS, where $P^* = \frac{a}{d} + \frac{\beta_2m}{ds_1} + \frac{c\delta pm}{d\mu_3s_2s_1}$, $S^* = \frac{m}{s_1}P^*$, $E^* = \frac{p}{s_2}S^*$, $M^* = \frac{\delta}{\mu_3}E^*$.

Proof. If $\delta > 0, p > 0, m > 0, a > -\frac{\beta_2m}{s_1} - \frac{c\delta pm}{\mu_3s_2s_1}$, then we obtain \mathcal{E}^* by a simple computation. The characteristic equation is

$$\lambda^4 + (\mu_3 + s_2 + s_1 + v_3)\lambda^3 + [\mu_3s_2 + (s_1 + v_3)(\mu_3 + s_2) + s_1v_3 - m\beta_2]\lambda^2 + [(s_1 + v_3)\mu_3s_2 + (s_1v_3 - m\beta_2)(s_2 + \mu_3)]\lambda + (s_1v_3 - m\beta_2)\mu_3s_2 - mcp\delta = 0,$$

$$v_3 = -a + 2dP^* = \frac{\beta_2m}{s_1} + \frac{c\delta pm}{\mu_3s_2s_1} + dP^* > \frac{\beta_2m}{s_1} + \frac{c\delta pm}{\mu_3s_2s_1}. \text{ Then we have } \Delta_1 = \mu_3 + s_2 + s_1 + v_3 > 0,$$

$$\Delta_2 = (\mu_3 + s_2)\mu_3s_2 + (\mu_3 + s_2 + s_1 + v_3)(s_1 + v_3)(\mu_3 + s_2) + (s_1 + v_3)(s_1v_3 - m\beta_2) > 0,$$

$$\begin{aligned} \Delta_3 &= (s_1 + v_3)(\mu_3 + s_2)\mu_3^2s_2^2 + (\mu_3 + s_2 + s_1 + v_3)(s_1 + v_3)^2(\mu_3 + s_2)\mu_3s_2 \\ &\quad + (s_1v_3 - m\beta_2)(s_1 + v_3)(\mu_3 + s_2)(\mu_3^2 + s_2^2 + (s_1 + v_3)(\mu_3 + s_2)) \\ &\quad + (s_1v_3 - m\beta_2)^2(s_1 + v_3)(\mu_3 + s_2) \\ &\quad + mcp\delta(\mu_3 + s_2 + s_1 + v_3)^2 > 0, \end{aligned}$$

$$\Delta_4 = ((s_1v_3 - m\beta_2)\mu_3s_2)\Delta_3 > 0.$$

By the Routh–Hurwitz criteria, \mathcal{E}^* (P^*, S^*, E^*, M^*) is LAS. ■

Theorem A.6. If $\delta \geq 0, p \geq 0, m \geq 0, a = -\frac{\beta_2m}{s_1} - \frac{c\delta pm}{\mu_3s_2s_1}$, then model (3.1) has a transcritical bifurcation at \mathcal{E}^0 .

Proof. For $a = -\frac{\beta_2m}{s_1} - \frac{c\delta pm}{\mu_3s_2s_1}$, the Jacobian matrix $J(\mathcal{E}^0)$ has zero eigenvalue. Thus, \mathcal{E}^0 is non-hyperbolic and $-\frac{\beta_2m}{s_1} - \frac{c\delta pm}{\mu_3s_2s_1}$ is the bifurcation value. Eigenvectors \mathbf{v} and \mathbf{w} of Jacobian matrices $J(\mathcal{E}^0)$ and $J(\mathcal{E}^0)^T$ corresponding to the zero eigenvalue are calculated as

$$\mathbf{v} = \left(\beta_2\mu_3s_1s_2 + c\delta p, \beta_2m\mu_3s_2 + c\delta pm, \frac{\beta_2m\mu_3s_2p + c\delta p^2m}{s_2}, \frac{\beta_2m\mu_3s_2\delta p + c\delta^2p^2m}{\mu_3s_2s_1} \right)^T,$$

$$\mathbf{w} = (\mu_3ms_2, \mu_3s_2, c\delta m, cms_2)^T.$$

Let $\mathbf{x} = (P, S, E, M)^T$, and denote model (3.1) as $\mathbf{x} = F(\mathbf{x}, a)$, where

$$F(\mathbf{x}, a) = \begin{pmatrix} aP + \beta_2S + cM - dP^2 \\ mP - s_1S \\ pS - s_2E \\ \delta E - \mu_3M \end{pmatrix}$$

Therefore,

$$F_a \left(\mathcal{E}^0, -\frac{\beta_2m}{s_1} - \frac{c\delta pm}{\mu_3s_2s_1} \right) = (0, 0, 0, 0)^T.$$

Direct calculations show that

$$\mathbf{w}^T F_a \left(\mathcal{E}^0, -\frac{\beta_2m}{s_1} - \frac{c\delta pm}{\mu_3s_2s_1} \right) = 0,$$

$$\mathbf{w}^T [DF_a \left(\mathcal{E}^0, -\frac{\beta_2m}{s_1} - \frac{c\delta pm}{\mu_3s_2s_1} \right) \mathbf{v}] = -\mu_3ms_2(\mu_3s_1s_2\beta_2 + c\delta p) < 0,$$

$$\mathbf{w}^T [D^2F \left(\mathcal{E}^0, -\frac{\beta_2m}{s_1} - \frac{c\delta pm}{\mu_3s_2s_1} \right) (\mathbf{v}, \mathbf{v})] = -2d\mu_3ms_2(\mu_3s_1s_2\beta_2 + c\delta p)^2 < 0.$$

By Sotomayor’s Theorem (Lawrence, 2001), the model (3.1) experiences a transcritical bifurcation at \mathcal{E}^0 . ■

Data availability

Data were obtained from public sources.

References

Benedetti-Cecchi, L., Canepa, A., Fuentes, V., et al., 2015. Deterministic factors overwhelm stochastic environmental fluctuations as drivers of jellyfish outbreaks. *PLoS One* 10 (10), e0141060.

Cabrales-Arellano, P., Islas-Flores, T., Thomé, P.E., et al., 2017. Indomethacin reproducibly induces metamorphosis in *Cassiopea xamachana* scyphistomae. *PeerJ* 5, e2979.

Chi, X., Zhang, F., Sun, S., 2022. Transgenerational effects and temperature variation alter life history traits of the moon jellyfish. *Front. Mar. Sci.* 9, 913654.

Condon, R.H., Duarte, C.M., Pitt, K.A., et al., 2013. Recurrent jellyfish blooms are a consequence of global oscillations. *Proc. Natl. Acad. Sci.* 110 (3), 1000–1005.

Conley, K., Uye, S.-i., 2015. Effects of hyposalinity on survival settlement of moon jellyfish (*Aurelia aurita*) planulae. *J. Exp. Mar. Biol. Ecol.* 462, 14–19.

Cui, Y., Sun, T., Zhang, J., et al., 2018. Influence of different material plastic plates on the planula larvae settlement of moon jellyfish *Aurelia* sp.1. *J. Appl. Oceanogr.* 37 (3), 366–371.

Dong, Z., Wang, F., Peng, S., et al., 2019. Effects of copper and reduced salinity on the early life stages of the moon jellyfish *Aurelia coerulea*. *J. Exp. Mar. Biol. Ecol.* 513, 42–46.

Duan, Y., Sun, M., Dong, J., et al., 2020. Effects of temperature on the growth asexual reproduction of moon jellyfish (*Aurelia coerulea*) polyps. *Acta Ecol. Sin.* 40 (13), 4404–4412, (in Chinese).

Duarte, C.M., Pitt, K.A., Lucas, C.H., et al., 2013. Is global ocean sprawl a cause of jellyfish blooms? *Front. Ecol. Environ.* 11, 91–97.

Efron, B., Tibshirani, R.J., 1994. *An Introduction to the Bootstrap*. Chapman Hall, New York, USA.

Feng, S., Wang, S.-W., Zhang, G.-T., et al., 2017. Selective suppression of *in situ* proliferation of scyphozoan polyps by biofouling. *Mar. Pollut. Bull.* 114 (2), 1046–1056.

Fuentes, V.L., Purcell, J.E., Condon, R.H., et al., 2018. Jellyfish blooms: advances and challenges. *Mar. Ecol. Prog. Ser.* 591, 3–5.

Gerber, N., Kokko, H., Ebert, D., et al., 2018. *Daphnia* invest in sexual reproduction when its relative costs are reduced. *Proc. R. Soc. B* 285 (1871), 20172176.

Goldstein, J., Steiner, U.K., 2020. Ecological drivers of jellyfish blooms—The complex life history of a ‘well-known’ medusa (*Aurelia aurita*). *J. Anim. Ecol.* 89 (3), 910–920.

Gröndahl, F., 1989. Evidence of gregarious settlement of planula larvae of the scyphozoan *Aurelia aurita*, an experimental study. *Mar. Ecol. Prog. Ser.* 56, 119–125.

Han, C.H., Uye, S.I., 2010. Combined effects of food supply and temperature on asexual reproduction and somatic growth of polyps of the common jellyfish *Aurelia* s.l. *Plankton Benthos Res.* 5 (3), 98–105.

Henschke, N., Stock, C.A., Sarmiento, J.L., 2018. Modeling population dynamics of scyphozoan jellyfish (*Aurelia* spp.) in the Gulf of Mexico. *Mar. Ecol. Prog. Ser.* 591, 167–183.

Hernroth, L., Gröndahl, F., 1985. On the biology of *Aurelia aurita* (L.) 3. Predation by *Coryphella verrucosa* (gastropoda, opisthobranchia), a major factor regulating the development of *Aurelia* populations in the gullmar fjord, western Sweden. *Ophelia* 24 (1), 37–45.

Hoover, R.A., Armour, R., Dow, I., et al., 2012. Nudibranch predation and dietary preference for the polyps of *Aurelia labiata* (Cnidaria: Scyphozoa). *Hydrobiologia* 690, 199–213.

Ishii, H., Katsukoshi, K., 2010. Seasonal and vertical distribution of *Aurelia aurita* polyps on a pylon in the innermost part of Tokyo Bay. *J. Oceanogr.* 66, 329–336.

Ishii, H., Ohba, T., Kobayashi, T., 2008. Effects of low dissolved oxygen on planula settlement, polyp growth and asexual reproduction of *Aurelia aurita*. *Plankton Benthos Res.* 3, 107113.

Kogovšek, T., Bogunović, B., Malej, A., 2010. Recurrence of bloom-forming scyphomedusae: wavelet analysis of a 200-year time series. *Hydrobiologia* 645, 81–96.

Kogovšek, T., Molinero, J.C., Lučić, D., et al., 2012. Interannual size changes of adult *Aurelia* sp.5 medusae stage in the Marine Protected Area of mljet IsSouth adriatic. *Acta Adriatica: Int. J. Mar. Sci.* 53 (2), 233–242.

- Kraus, J.E.M., Fredman, D., Wang, W., et al., 2015. Adoption of conserved developmental genes in development and origin of the medusa body plan *EvoDevo* 6, 23.
- Lawrence, P., 2001. *Differential Equations and Dynamical Systems*, third ed. Springer, New York, pp. 338–339.
- Li, C., Liu, H., 2022. Exploring cosmopolitan jellyfish (*Aurelia* spp.) bloom dynamics and ecological implications in subtropical waters with mechanistic dynamic modeling *J. Mar. Syst.* 228, 103705.
- Lucas, C.H., 1996. Population dynamics of *Aurelia aurita* (scyphozoa) from an isolated brackish lake, with particular reference to sexual reproduction *J. Plankton Res.* 18 (6), 987–1007.
- Lucas, C.H., 2001. Reproduction and life history strategies of the common jellyfish, *Aurelia aurita*, in relation to its ambient environment *Hydrobiologia* 451, 229–246.
- Lucas, C.H., Graham, W.M., Widmer, C., 2012. Jellyfish life histories: Role of polyps in forming and maintaining scyphomedusa populations *Adv. Mar. Biol.* 63, 133–196.
- Luo, J.H., 2013. Phytoplankton-zooplankton dynamics in periodic environments taking into account eutrophication *Math. Biosci.* 245 (2), 126–136.
- Marelli, S., Lamas, C., Konakli, K., et al., 2022. UQLab user manual – Sensitivity analysis Chair of Risk, Safety and Uncertainty Quantification, ETH Zurich, Switzerland.
- Marelli, S., Sudret, B., 2014. UQLab: A framework for uncertainty quantification in Matlab In: *Proc. 2nd Int. Conf. on Vulnerability, Risk Analysis and Management (ICVRAM2014)*. Liverpool, United Kingdom, pp. 2554–2563.
- Marques, R., Darnaude, A.M., Schiariti, A., et al., 2019. Dynamics and asexual reproduction of the jellyfish *Aurelia coerulea* benthic life stage in the thau lagoon (northwestern Mediterranean) *Mar. Biol.* 166, 74.
- Miyake, H., Terazaki, M., Kakinuma, Y., 2002. On the polyps of the common jellyfish *Aurelia aurita* in Kagoshima Bay *J. Oceanogr.* 58 (3), 451–459.
- Purcell, J.E., 2005. Climate effects on formation of jellyfish and ctenophore blooms: a review *J. Mar. Biol. Assoc. UK* 85 (3), 461–476.
- Purcell, J.E., 2012. Jellyfish and ctenophore blooms coincide with human proliferations and environmental perturbations *Annu. Rev. Mar. Sci.* 4, 209–235.
- Purcell, J.E., Hoover, R.A., Schwarck, N.T., 2009. Interannual variation of strobilation by the scyphozoan *Aurelia labiata* in relation to polyp density, temperature, salinity, and light conditions *in situ* *Mar. Ecol. Prog. Ser.* 375, 139–149.
- Purcell, J.E., Uye, S., Lo, W., 2007. Anthropogenic causes of jellyfish blooms and their direct consequences for humans: a review *Mar. Ecol. Prog. Ser.* 350, 153–174.
- Rahi, J.E., Weeber, M.P., Serafy, G.E., 2020. Modelling the effect of behavior on the distribution of the jellyfish mauve stinger (*Pelagia noctiluca*) in the Balearic Sea using an individual-based model *Ecol. Model.* 433, 109230.
- Roveta, C., Annibaldi, A., Domenichelli, F., et al., 2022. Single and combined effects of two trace elements (Cd and Cu) on the asexual reproduction of *Aurelia* sp. polyps *Aquat. Ecol.* 56, 631–637.
- Ruiz, J., Prieto, L., Astorga, D., 2012. A model for temperature control of jellyfish (*Cotylorhiza tuberculata*) outbreaks: A causal analysis in a Mediterranean coastal lagoon *Ecol. Model.* 233, 59–69.
- Schiariti, A., Melica, V., Kogovšek, T., et al., 2015. Density-dependent effects control the reproductive strategy and population growth of *Aurelia aurita* s.l. scyphistomae *Mar. Biol.* 162, 1665–1672.
- Shi, Y., Yu, Z., Zhen, Y., et al., 2018. Effect of decreasing temperature on the strobilation of *Aurelia* sp.1 *J. Oceanol. Limnol.* 36 (2), 465–472.
- Sun, M., Chai, Y., Dong, J., et al., 2017. Effects of environmental factors on polyp survival reproduction of *Aurelia* sp.1 *Acta Ecol. Sin.* 37 (4), 1309–1317, (in Chinese).
- Sun, S., Sun, X., Zhang, G., et al., 2011. Long-term changes in major meteorological and hydrological factors in the Jiaozhou Bay *Oceanol. Limnol. Sin.* 42 (5), 632–638, (in Chinese).
- Takao, M., Okawachi, H., Uye, 2014. Natural predators of polyps of *Aurelia aurita* s.l. (Cnidaria: Scyphozoa: Semeaostomeae) and their predation rates *Plankton Benthos Res.* 9, 105–113.
- Tiller, R.G., Borgersen, Å.L., Knutsen, Ø., et al., 2017. Coming soon to a fjord near you: future jellyfish scenarios in a changing climate *Coast. Manage.* 45 (1), 1–23.
- Treible, L.M., Condon, R.H., 2019. Temperature-driven asexual reproduction and strobilation in three scyphozoan jellyfish polyps *J. Exp. Mar. Biol. Ecol.* 520, 151204.
- Uye, S., Shimauchi, H., 2005. Population biomass, feeding, respiration and growth rates, and carbon budget of the scyphomedusa *Aurelia aurita* in the Inland Sea of Japan *J. Plankton Res.* 27 (3), 237–248.
- Wan, A., Zhang, G., 2012. Annual occurrence of moon jellyfish *Aurelia* sp. 1 in the jiaozhou bay its impacts on zooplankton community *Oceanol. Limnol. Sin.* 43 (3), 494–501, (in Chinese).
- Wang, Y.T., 2013. *Study on the Key Processes of Life Cycle of Aurelia Sp. 1* (). (Ph.D. thesis). Institute of Oceanology, Chinese Academy of Sciences, (in Chinese).
- Wang, N., Li, C., Liang, Y., et al., 2015. Prey concentration and temperature effect on budding and strobilation of *Aurelia* sp 1 polyps *Hydrobiologia* 754 (1), 125–134.
- Wang, Y.T., Sun, S., 2015. Population dynamics of *Aurelia* sp.1 ephyrae and medusae in Jiaozhou Bay, China *Hydrobiologia* 754 (1), 147–155.
- Willcox, S., Moltchanivskyj, N.A., Crawford, C.M., 2008. Population dynamics of natural colonies of *Aurelia* sp. scyphistomae in Tasmania, Australia *Mar. Biol.* 154, 661–670.
- Xie, C., Fan, M., Kang, Y., 2021. Population dynamics of the giant jellyfish *Nemopilela nomurai* with age structure *Ecol. Model.* 441, 109412.
- Xie, C., Fan, M., Wang, X., et al., 2015. Dynamic model for life history of scyphozoa *PLoS One* 10 (6), e0130669.
- Xing, Y., Liu, Q., Zhang, M., et al., 2020. Effects of temperature and salinity on the asexual reproduction of *Aurelia coerulea* polyps *J. Oceanol. Limnol.* 38 (1), 133–142.
- Yu, S., Song, D., Fan, M., et al., 2023. Effects of temperature and salinity on growth of *Aurelia aurita* *Ecol. Model.* 476, 110229.
- Zang, W., Zhang, F., Chi, X., et al., 2022. Relationship between asexual reproduction of *Aurelia coerulea* polyps and jellyfish blooms under the influence of temperature dynamics in winter and spring *Front. Mar. Sci.* 9, 2296–7745.
- Zang, W., Zhang, F., Sun, Y., et al., 2023. Benthic ecosystem determines jellyfish blooms by controlling the polyp colony development *Mar. Pollut. Bull.* 193, 115232.
- Zheng, F.Y., Chen, S.Q., Ni, J., 2010. Biological characteristics of moon jellyfish (*Aurelia aurita* Linnaeus, 1758) and its bloom *Adv. Mar. Sci.* 28 (1), 126–132, (in Chinese).